

# 1. FUNCTIONAL NEUROIMAGING: AN INTRODUCTION TO THE TECHNOLOGY, METHODOLOGY, INTERPRETATION, AND APPLICATIONS

Tamara A Russell, Fernando Zelaya, Rodrigo A  
Bressan, Peter A Bandettini

## *Introduction*

---

Many technological advances have been seen in the neuroimaging field. These advances are allowing the investigation of new and exciting neurophysiological and pathophysiological questions. This chapter intends to provide the reader with a brief overview of the principles of MRI, fMRI, PET and SPET. Basic information on the hardware, specific applications and major limitations of the different neuroimaging techniques is provided to give the reader a perspective of what can and cannot be done with these techniques. Functional magnetic resonance imaging (fMRI) has been in existence for about 11 years.<sup>1-3</sup> During this time, the technique has experienced explosive growth. The reasons for this growth include the following: minimal invasiveness; the growing availability of the necessary hardware; the unique functional spatial and temporal resolution niche that it fills; its ability to map a network of substrates that intervenes in cognitive and sensory processes; and, importantly, the potential that it promises for the investigation of abnormal brain function. Figure 1.1 is an attempt to graphically illustrate a timeline of the advancement of many, but certainly not all, significant aspects of functional imaging technologies.

Although the use of this tool has increased exponentially, it is still quite difficult for the average end-user, perhaps a psychologist or psychiatrist, to come to grips with the basic principles and physics of MR. The aim of the first section of this chapter is to provide an overview of these basic principles. Subsequent sections will describe aspects of the hardware used in the MRI environment, and advances and developments that are being made in

NEUROIMAGING IN PSYCHIATRY

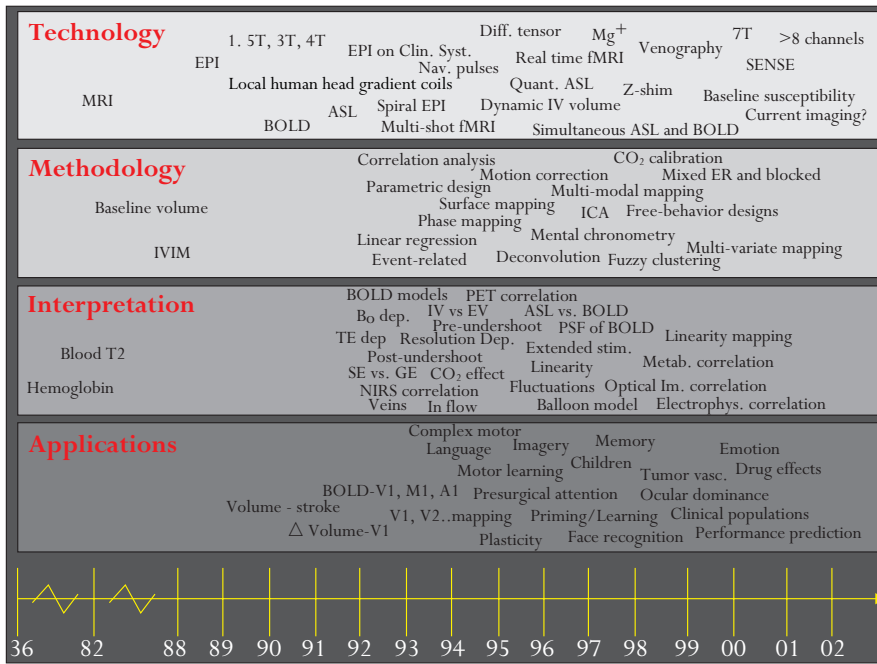


**Figure 1.1** Growth and progression of neuroimaging techniques. *A1*, auditory cortex; *ASL*, arterial spin labeling;  $B_0$ , external field; *BOLD*, blood oxygenation-level dependent; *EPI*, echo planar imaging; *ER*, event related; *EV*, extravascular; *fMRI*, functional magnetic resonance imaging; *GE*, gradient echo; *ICA*, independent component analysis; *IV*, intravenous; *IVIM*, intravoxel incoherent motion; *IV v EV*, intravascular versus extravascular; *M1*, motor cortex; *MRI*, magnetic resonance imaging; *NIRS*, near infrared spectroscopy; *PSF*, point spread function; *SE*, spin echo; *SENSE*, sensitivity encoding for fast MRI; *T*, tesla; *V1*, visual area 1; *V2*, visual area 2.

this area. Additionally, some discussion of the neuronal information extracted from the blood oxygenation-level-dependent (BOLD) signal will be discussed. Lastly, the applications of this tool are briefly outlined.

### Basic principles of functional magnetic resonance imaging (fMRI)

fMRI is a new application of an existing technology (i.e. MRI). This section will attempt to introduce, in a basic way accessible to the novice, the elements involved in the production of the MRI signal. It will cover basic principles relating to the nuclei of hydrogen atoms (which is where most of the

MR signal comes from) and their properties when an external magnetic field is applied. Precession and resonance will be described, as will the mechanisms by which protons can be excited and relaxed. By necessity, in order to provide a brief introduction to this area, some aspects of this explanation may be deemed by the more experienced reader as oversimplified. It is stressed at this point that the purpose of this chapter is to provide an introductory overview to the novice neuroimager, providing a level of understanding that will demystify some of the principles and terminology used, not to provide an in-depth understanding of all the physics involved in MRI.

### **Nucleus of the hydrogen atom**

Hydrogen atoms give rise to most of the signal in an MR image. The nucleus of the hydrogen atom consists of one proton and no neutrons. This gives the hydrogen atom a positive charge and an atomic number of 1, as there is only one proton in its nucleus. Hydrogen atoms are abundant in the human body: approximately 70% of the body is made up of water (containing two hydrogen atoms and one oxygen atom). In the brain, gray matter has approximately a 70% water content, blood approximately a 93% water content and white matter (glial cells) approximately an 85% water content. The large quantity of hydrogen atoms in the human body and the large magnetic moment (see below) of the single proton in the nucleus of the atom are responsible for the large MR signal they produce when compared with those of other nuclei.

### **Magnetic moment**

Some atomic nuclei have the property of 'spin'. This means that they have a *net* angular momentum, i.e. they can be seen as 'rotating' around their main axis. The spinning protons combined with their net electric charge create what is called a net magnetic moment, as if they were a small magnet with a north and a south pole.

### **External magnetic fields**

In the absence of any external magnetic field, proton magnetic moments are randomly orientated and (as a group) are considered to have a net magnetization of zero. When an external magnetic field is applied to an object, the spin axes of all the nuclei in the object line up with the magnetic field. The nuclei can either align *parallel* to the magnetic field or *anti-parallel* to it (i.e. in the opposite direction). Factors which influence the direction of orientation include the thermal energy of the atoms and the strength of the external magnetic field. High-energy protons are strong enough to be able to align

themselves anti-parallel to the external magnetic field while those with low energy will align in a direction parallel to the magnetic field. In reality, the number of protons that align parallel and anti-parallel with the field is not the same. This difference produces a net magnetization of the whole sample (in our case, the human brain). With increases in magnetic field strength, this difference increases, therefore enhancing the net magnetization of the sample.

For simplicity, it is easier to consider from here onwards only the *net* magnetization of the sample. As you may have realized, this net magnetization has a definite orientation, i.e. in the direction of the excess of protons that align parallel with the field. Therefore, it is represented as a vector quantity, which is termed the *net magnetization vector* (NMV) or  $M$ .

### Precession

Because of their intrinsic angular momentum (described above), protons do not align with the external field (parallel or anti-parallel) in a 'straight' line. Instead, they behave just like a spinning top does as it starts to fall. *Precession* is the term used to describe the way in which protons 'wobble' around their axes. When an external magnetic field is applied, the protons precess in line with it, but wobble in a conical manner that is similar to the spinning top rotating around a vertical axis. *Precessional frequency* is a term used to describe the rate (or speed) at which the protons or the NMV precesses.

### Resonance and the Larmor frequency

When exposed to an external magnetic field, all hydrogen protons will precess at the same frequency. This frequency is determined by the gyromagnetic ratio of the particular protons and the strength of the magnetic field. It is described by a very simple equation called the Larmor equation, which states that the frequency of precession ( $\omega$ ) is given by the product of the gyromagnetic ratio of the protons ( $\gamma$ ) times the strength of the external field ( $B_0$ ):

$$\omega = \gamma B_0$$

The gyromagnetic ratio of hydrogen is 42.57 MHz/tesla (T) and all hydrogen protons will precess at this same frequency when exposed to an external magnetic field of 1 T. The strength of the magnetic field (from the scanner) is measured in tesla (T) or gauss (G): 1 T is equivalent to  $1 \times 10^4$  G (about 20,000 times stronger than the earth's magnetic field).

As can be seen, this equation determines the frequency at which the protons will resonate. The resonant frequency is also referred to as the

*precessional frequency* or the *Larmor frequency*. The equation also demonstrates that the higher the magnetic field, the greater the precessional frequency.

The strength of the magnetic field will usually increase the intensity of the signal because the net magnetization will be larger. It is also worth noting that fMRI contrast also increases approximately linearly with field strength.<sup>4-6</sup> Field strength drives both the frequency of precession of protons and the fMRI contrast in a linear fashion. The drive for an increased signal:noise ratio (S:N; i.e. the height of the signal of interest compared to the background noise) and for increased functional contrast has been responsible for the proliferation of higher field strength magnets for human fMRI, from typically 1.0 T in 1984 to the present day where scanners in the range of 4–7 T are being developed for human use. Field strengths as high as 12 T are being developed for animal use. The majority of scanners in use in academic centers are in the range of 1.5–4 T. Higher field magnets cost more to build and maintain, and create their own technical hurdles. Some of the advantages and disadvantages of high field strength are outlined in Table 1.1.

But what actually is *resonance*? Resonance refers to the property of a body (in this case the nucleus of an atom) to absorb energy at a characteristic, natural frequency. In MR, the natural frequency for resonance absorption is given by the Larmor equation. A condition of resonance can be achieved by placing the protons within a strong external field and exciting them with a second, alternating magnetic field [in the form of radiofrequency (RF) waves, see below]. When resonance occurs, not only do the magnetic moments of the protons change their angle of rotation, but all the protons begin to precess in phase with each other (referred to as *phase coherence*).

Protons can absorb energy from external sources but also give off energy when they try to change their alignment back to their initial configuration in the magnetic field. These two types of processes form the basis of how the MR signal is created and how it disappears.

Noll<sup>7</sup> has described the resonance phenomena using the analogy of a guitar string. With a guitar, the frequency varies according to how much tension is applied to the string by the fingers [similar to the strength of the magnetic field ( $B_0$ )]. The string is most often plucked in order to excite it and create resonance (in the form of acoustic waves), however, it can also be excited by holding up a loudspeaker near to the string and playing a note *at the same frequency* as the string. This is similar in manner to the way in which nuclear spins are excited by the application of RF waves (a second, alternating magnetic field of the correct frequency).

## NEUROIMAGING IN PSYCHIATRY

<b>Table 1.1 Advantages and disadvantages of high field strength functional magnetic resonance imaging (fMRI)</b>	
<i>Advantages</i>	<i>Disadvantages</i>
Signal to noise (S:N) is linearly proportional to field strength	In fMRI what matters is temporal signal to noise, which does not scale with field strength at typical (low) resolutions since physiologic fluctuations, independent of field strength, contribute significantly. This will blunt external field ( $B_0$ )-based gains in S:N ratios and functional contrast to noise
Functional contrast to noise increases with $B_0$ , allowing comparisons of more subtle signal changes or for shorter scans for similar quality functional maps	Baseline $T2^*$ and $T2$ also decrease with $B_0$ , therefore lowering the time interval between the radiofrequency (RF) pulse and the middle echo (TE) at which optimal contrast is obtained, reducing the gain in functional contrast to noise somewhat
High S:N ratio allows higher resolutions to be obtained	To achieve high resolutions, one needs a longer readout window (difficult at higher field strengths) or multishot imaging (time consuming and more temporally unstable)
Blood $T1$ increases, increasing functional contrast for arterial spin labeling (ASL) perfusion imaging techniques. It is thought that at just above 7 T, perfusion and blood oxygenation-level dependent (BOLD) functional contrasts are similar	At typical fMRI resolutions, signal dropout is greater at higher field strengths, requiring better shimming techniques and/or smaller voxel sizes
At field strengths $\geq 3$ T, vein $T2^*$ becomes much less than gray matter $T2^*$ , making the creation of venograms a simple matter of collecting a high-resolution $T2^*$ scan	RF power deposition issues are more significant at higher field strengths, therefore limiting continuous ASL techniques and high-resolution fast spin-echo imaging.
At field strengths $\geq 9$ T, the intravascular contribution is zero, therefore enabling more precise functional localization	It is more difficult to create a homogeneous RF power deposition at higher field strengths

The term *excitation* is used to describe the delivery of energy to the protons at their characteristic frequency. As the proton resonates it moves out of alignment with the external magnetic field ( $B_0$ ), to attempt to align with the second, alternating magnetic field. The NMV is now also changing

out of alignment with  $B_0$ . This alternating magnetic field is delivered in the form of a pulse. The length of the pulse will determine the *flip* angle (in degrees) by which the net magnetization is tilted away from  $B_0$ . If a pulse is applied to produce a rotation of  $90^\circ$  then, eventually, all the protons that were aligned with  $B_0$  will change their alignment so that they are precessing in what is called the *transverse plane* (at  $90^\circ$  to  $B_0$ ). Similarly, if a flip angle of  $180^\circ$  is used, then the precession and alignment of the protons will eventually be anti-parallel to the original magnetization direction. Maximum detection is obtained with a flip angle of  $90^\circ$ .

Once the protons have been 'flipped' by the external energy source (in this case RF pulse) and the pulse is terminated, the protons will start to relax and begin to attempt to realign with  $B_0$ . This process will take a finite period of time and will evolve with a time constant referred to as T1. T1 is dependent on the physical and chemical properties of the environment in which the protons are residing. The time between successive RF pulses (TR) will determine the optimum flip angle for the experiment. For a given value of TR, the shorter T1, the larger the flip angle which can be used between successive excitations.

### Relaxation of excited protons

In general terms, T1 is the time constant with which protons will reach their equilibrium magnetization. As mentioned above, T1 is roughly the time it takes for the protons to change their alignment from the transverse plane back to the original direction  $B_0$ . This is also called longitudinal relaxation. As T1 occurs, another separate, but simultaneous, phenomena called T2 occurs. This is the transverse relaxation time, or T2 decay, which is the natural decay of the signal in the transverse plane. It is also referred to as T2 relaxation time, T2 decay or 'spin-spin relaxation time'. It is observed that when the RF pulse is terminated, those protons precessing in the transverse plane will gradually begin to realign with  $B_0$  and, at the same time, the signal will decay. The decay is caused by both the return to equilibrium and the transverse relaxation (with a time constant of T2). Like T1, T2 decay is also dependent on the interactions the spins have with each other and with their microenvironment, i.e. the tissue that they are in, e.g. fat or water. Some spins might decay more quickly than others. The longer TR is, the more the protons in the transverse plane decay and begin to lose phase coherence (i.e. they will no longer be spinning at the same frequency or in the same plane). An important concept to note is that, strictly speaking, the term T2\* is the term

used to describe the time constant with which the detected signal decays. This reduction of signal in the transverse plane is primarily caused by the fact that the magnetic field is not precisely the same in all parts of the sample, i.e. the field is inhomogeneous. From the Larmor equation, it can be seen that since these differences in field will give rise to differences in the Larmor frequencies at each point in space, the precession of protons at different rates will make them lose phase coherence, thus destroying the signal. Therefore  $T2^*$  is shorter than the natural decay,  $T2$ .

### **Tissue contrast**

Signals given out over the course of manipulations with RF pulses depend on the local microenvironment surrounding the proton; e.g. hydrogen nuclei in fats transmit different radio signals compared to those in water. This property allows the signal obtained to be used to distinguish between different tissues in the body, or create contrast. Due to the  $T1$  and  $T2$  relaxation properties, it is possible to differentiate between various tissues in the body: this is called *contrast*.

Fat nuclei have a slow molecular motion and longitudinal relaxation ( $T1$ ) occurs rapidly. Therefore, the time it takes for the NMV to realign with  $B_0$  in fat is short. In contrast, water molecules have a high mobility, which means that the proton–proton interactions between water nuclei (which also contribute to the decay of the signal) are averaged towards zero, and hence it takes longer for them to realign with  $B_0$ , i.e. they have a long  $T1$ . With respect to  $T2$  decay, fat has a very efficient energy exchange with its surrounding tissue and therefore it can very quickly give up the energy it has absorbed to neighboring cells, leading to a short  $T2$ . Water, on the other hand, is less efficient and has a longer  $T2$ .

The concept of contrast can also be extended to other types of differentiations between proton signals. One of the reasons for the widespread use of MRI is the fact that it can also be used to differentiate between healthy and pathologic tissue by examining their differences in mobility, composition, etc. As will be seen later, in fMRI these concepts are used to create contrast between active and less active sites of brain activity.

### **Summary**

- Protons (i.e. the nuclei of hydrogen atoms) are randomly aligned in the body.
- An applied external magnetic field ( $B_0$ ), measured in tesla (T), comes from the magnet of the scanner.

- Protons align either parallel or anti-parallel to  $B_0$ , and the difference between these two populations gives the net magnetization vector (NMF).
- Protons precess or wobble around the axis of this magnetic field.
- A radiofrequency (RF) pulse at the Larmor frequency for hydrogen is applied, which causes protons to tilt away from the direction of the applied field.
- The duration of the RF pulse will determine the angle by which the protons will tilt away from the field.
- The MR signal is detected by tilting the magnetization towards the direction of a receiver coil.
- When the RF is terminated, protons de-phase and lose their coherence, and try to realign with  $B_0$ .
- Proton realignment (T1) and longitudinal (T2) relaxation occur simultaneously.

## *Magnetic resonance imaging hardware*

The section above has attempted to describe, in a simply way, some of the basic principles behind the MR signal and how it is obtained. To a certain extent, these principles are invariant, i.e. they are physical facts that cannot be manipulated. In order to gain optimum use of the natural contrast that occurs as the result of magnetization of the human brain, certain tools or hardware are used and manipulated by MR physicists. It is here that a degree of variation can be introduced in order to optimize the signal that is received.

This section describes some of the tools at the disposal of the physicist and, additionally, some of the new directions that can be taken with various manipulations to take fMRI forward, e.g. gradient coils, different pulse sequences and RF receiver coils.

### **Gradient coils**

The component of the imaging system that allows the spatial localization of the protons is a set of *magnetic field gradients*, set up by magnetic coils which are turned on and off. Coils are used to apply magnetic field gradients within the larger magnetic field of the scanner magnet. Their purpose is to make the Larmor frequencies of the sample proportional to their position in space.

*How is a slice selected?*

A magnetic field gradient along the  $z$ -axis, also called the slice-select gradient, is normally turned on at the same time that the first RF pulse is applied. For example, with a 2 T system, a gradient of 0.1 T/cm may be set up along the  $z$ -axis. This would mean that, at the center of the magnet, the amplitude of the magnetic field was 2 T. But, along the  $z$ -direction, the value of the magnetic field ( $B_0$ ) will increase or decrease by 0.1 T/cm. This gradient causes hydrogen nuclei at one end of the magnet to precess at a higher frequency (more than the Larmor frequency) and those at the other end (weaker magnetic field) to precess at a lower frequency (less than the Larmor frequency). Remember (as described earlier under Resonance and the Larmor frequency) that resonance only occurs when protons are excited at their own frequency, as determined by the Larmor equation. For example, if a gradient was set up that caused protons to precess at 63 MHz at one end of the magnet (this could be at the feet of the subject) up to 65 MHz at the other end (the head of the subject), then a 65 MHz RF pulse would excite nuclei in a slice near the head of the subject but not near the feet; conversely, a 63 MHz pulse would excite nuclei near the feet of the subject and not at the head. Thus, a single 'slice' of the gradient can be excited depending on the frequency at which the RF pulse is delivered. Only the protons in that slice will be excited. Other slices can be excited by shifting either the frequency of the RF pulse up or down, or by shifting the overall magnetic field up or down. This gradient will, however, only give spatial information in one dimension.

The width of the selected slice will be given by the particular characteristics of the RF pulse that is employed, and the magnitude of the slice-select gradient. 'Shaped' pulses (where the RF envelope has a special shape) are employed which select only a band of frequencies. The amplitude of the gradient then determines the spatial thickness that the band of frequencies corresponds to.

*Encoding the information in the plane of the image*

The previous section showed how to select a 'slice' of protons anywhere in the volume of the magnet, but what is wanted is the anatomical detail in the plane of the image. In other words, the Larmor frequencies of the protons of the slice in the remaining two dimensions (if the slice was selected across the  $z$ -direction, then the plane of the slice would be in the  $xy$ -plane) need to be encoded.

This is done by using two additional field gradients, one that linearly varies the Larmor frequencies along  $x$ -plane and the other that does the

same thing along the  $y$ -plane. The actual manner in which this process of frequency encoding is done can be made in literally hundreds of ways. For simplicity, described here is the simplest scenario. In this context, the situation is similar to that described above, i.e. the frequencies of the protons will depend on their position along  $x$  by turning on a linear gradient along the  $x$ -axis (hence, protons at one end of the  $x$ -axis of the magnet will precess faster than protons at the other end).

The important distinction from the process of slice selection is that in this part of the acquisition process we will actually *detect* the MR signal in the presence of the  $x$ -gradient. This means that the signal captured contains contributions from *all* of the protons in the selected slice, but the individual frequencies that contribute to it have a signature of where they come from in the  $x$ -direction by virtue of the gradient applied. This is what is meant by frequency encoding along  $x$ . Note that all that has been achieved so far is to select a slice and to give that slice an amount of frequency encoding, there is still not enough information to create an image. All we have is a projection of all the points of the slice along the  $x$ -axis.

What about the other dimension (i.e.  $y$ )? This second dimension could be encoded in exactly the same manner, i.e. in principle, two linear gradients could be turned on along  $x$  and  $y$  simultaneously, and the signal captured in the presence of both of them. The resulting signal would correspond to a projection of the entire slice along a line defined by the vector sum of the  $x$ - and  $y$ -gradients. This could be repeated many times for various values of the  $x$ - and  $y$ -gradients until enough frequency information for the entire sample was defined. Indeed, this is how MRI was first performed in 1973, when it was called projection reconstruction.<sup>8</sup>

However, a more efficient way of encoding the second dimension is to do the process in two stages. Firstly (after selecting the slice), a gradient is turned on in the  $y$ -dimension for a finite amount of time, but the MR signal is *not* detected in its presence; some quantity of frequency encoding to the protons have simply been assigned depending on their position along  $y$ . Some time after the  $y$ -gradient pulse, a gradient is turned on in the  $x$ -direction, but this time the signal is detected in the presence of the  $x$ -gradient. So, the signal detected carries contributions from the frequencies of all protons according to their position in  $x$  but, because of the preceding  $y$ -gradient pulse, their relative phase is different depending on their position along  $y$ . The  $y$ -gradient has therefore achieved the function of *phase encoding* the signals and the  $x$ -gradient has provided the role of *frequency encoding*.

NEUROIMAGING IN PSYCHIATRY

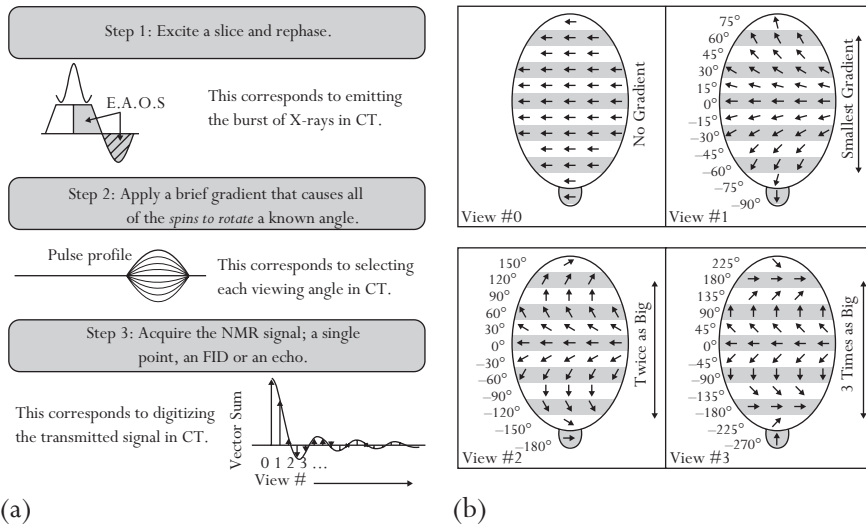


**Figure 1.2** (a) Schematic representation of the principle of 'spin-warp' phase encoding. In Step 2, a different magnitude of the phase encoding gradient is applied for each 'view'. This makes all the spins in the sample rotate by a known angle. In Step 3, the signal that is captured immediately has a relative phase difference which is directly proportional to the amplitude and duration of that gradient. (b) The effect of the phase encoding gradient on each one of the 'views'. The signal acquires a relative phase evolution along the vertical direction which is dependent upon its position. Notice that along the horizontal direction all spins possess the same phase angle. (Reproduced from NessAiver. All you need to know about MRI physics, University of Maryland, Medical Centre with permission from Moriel NessAiver, Simply Physics.)

In practice, the process detailed above is repeated several times for different values of the  $y$ -gradient until all the frequency encoding (see Figure 1.2) in both dimensions has been achieved.

*Decoding the signal*

Although the processes leading to the complete encoding of three-dimensional information on the MR signal have been described, the issue of how this information is decoded in order to produce the two-dimensional image has not been addressed.

In order to achieve this, an operation called Fourier transformation (FT) is used. This literally transforms the signals from the time domain in which they are acquired to a frequency domain, which, as has been shown, is equivalent to their position in space because the magnitude of frequency encoding applied along the  $x$ - and  $y$ -directions is known. The FT gives, for each signal, the spectrum of frequencies that make up that signal. In simple

terms, once it is known which signal amplitudes correspond to which frequencies, then the frequency is converted to spatial coordinates from the magnitude of the applied gradient.

Fourier transformation is one of various types of transform operations that can take us from one domain to another, in this case from time to frequency (i.e. space). FT is performed because there are readily available algorithms which allow most computers to perform this function very quickly.

Nowadays, there are literally hundreds of schemes for frequency and phase encoding. The ones of interest for functional imaging are those which can be performed very quickly, so as to provide good temporal resolution in the evaluation of cognitive and sensory processes. The fast imaging method of choice is echo planar imaging (EPI), a technique in which *all* the necessary frequency and phase encoding information is generated from a single excitation. This means that one complete two-dimensional slice can be collected in approximately 100 ms. (As will be seen later, the second criterion for choosing an imaging modality for functional studies is the manner in which the *contrast* of the image is tailored to reflect the differences between states of activity.)

#### *Different acquisition techniques*

The rate of image acquisition is primarily limited by how rapidly the gradients can be switched on and off, and how long the signal lasts whilst it is being digitized.

From the point of view of how all the information necessary to construct the image is collected, MRI can be divided into *single-shot* and *multishot* techniques. In single-shot techniques, all the data necessary for creation of an image are collected (read) in one single time window, or in a series of small time windows within the same repetition time. The information arises only from samples of longitudinal magnetization. As mentioned above, EPI is one such single-shot technique in that one 'plane' of data is collected after the application of a single RF pulse (gradient-echo EPI) or two RF pulses (spin-echo EPI).

The temporal domain in which signals are collected (in the presence of the frequency-encoding gradient) is often called the *k*-space, a term that arose because of the similarities between MRI and diffraction (and crystallography<sup>9</sup>). The *k*-space is simply a convenient coordinate system in which the raw data is represented, but it also has the property that it corresponds to the inverse space of the object. So, in order to collect all the information to make the image, we simply have to collect the minimum number of *k*-space points needed to be inverted by FT (mentioned above) to generate the image of the object.

In single-shot EPI, all the  $k$ -space points that make the image are collected in one repetition time. In multishot EPI, various parts of  $k$ -space are collected sequentially in different repetition times. Higher image quality is obtained in this manner but a large penalty is paid in terms of acquisition time, which is why multishot techniques are not generally used for functional imaging studies.

In multishot MRI, a single 'line' (in  $k$ -space) of raw data is acquired with each excitation pulse. Because of the relatively slow rate at which the magnetization returns to equilibrium following excitation (determined by  $T_1$  of the particular tissue), a certain amount of time is required between shots, otherwise the signal would rapidly be saturated. Because of this required recovery time (at least 150 ms for gray matter protons at 1.5 T), multishot techniques are typically slower than single-shot techniques. For a 150 ms TR (elapsed time between successive RF excitation pulses), a multishot image with 128 lines of raw data would take  $150 \text{ ms} \times 128 = 19.2 \text{ s}$ .

In the case of EPI, the entire data set for a single plane is typically acquired in about 20–40 ms. For an fMRI experiment, the time interval between the RF pulse and the measurement of the middle echo (TE) is about 40 ms. Along with some additional time for applying other necessary gradients, the total time for an image to be acquired is about 60–100 ms, allowing 10–16 images to be acquired in 1 s (one image in 100 ms = 10 images in 1000 ms). Improvements in digital sampling rates and gradient slew rates (how fast a gradient can be turned on and off to different field strengths) will allow further gains in this number, but, essentially, this is about the upper limit for imaging humans.

In the context of an fMRI experiment with EPI, the typical image acquisition rate (for the whole brain volume) is also determined by how many slices can temporally fit into TR. For whole brain imaging, approximately 20 slices (5 mm thickness) are typically required to cover the entire brain. This would allow a TR of about 1.5–2 s at minimum. This image sampling rate is often adequate to capture most of the details of the slow and dispersed activation-related hemodynamic response, which takes about 12 s to completely evolve. The basic dynamics of the signal are shown in Figure 1.3.

Image *spatial* resolution is also primarily determined by the gradient strength, the digitizing rate, and the time available. For multishot imaging, higher resolution images can be achieved at the expense of prolonged imaging times. But note that these techniques become unsuitable for *functional* imaging studies since, in most instances, we want to improve the temporal resolution of the functional examination and, as is the case in

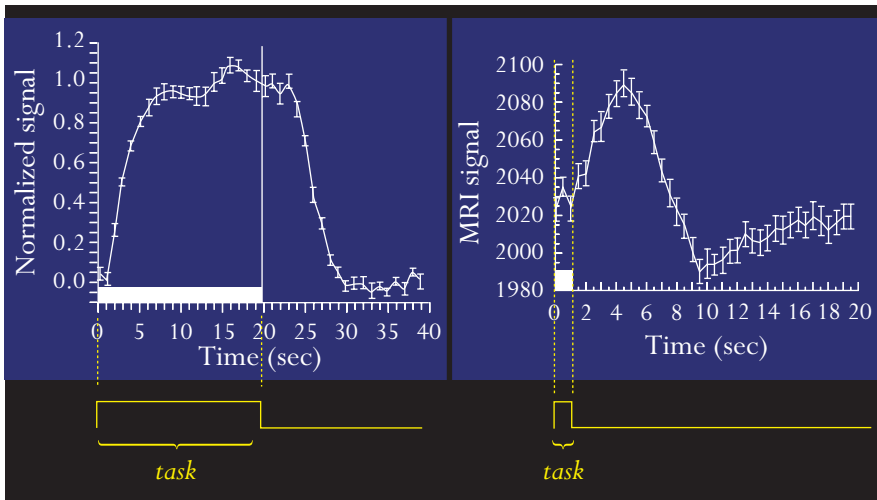


**Figure 1.3** Basic dynamics of the magnetic resonance imaging (MRI) signal.

event-related investigations, preserve the ability to assign at least one volume to every stimulus that is presented.

In EPI, all the gradient pulses necessary to define the image matrix in two dimensions are applied following a single excitation (i.e. one RF pulse). The frequency encoding is achieved by successive reversals of one of the gradients (normally called the *read* gradient). In other words, the gradient waveform looks like a series of positive and negative lobes. This gives rise to a series of gradient echoes in the middle of each one of the lobes, and each echo is used to encode one line of *k*-space along the read (frequency-encoding) direction.

Prior to each frequency gradient lobe, a small gradient (a blip) is applied along the other (orthogonal) direction of the image, which effectively shifts the position of each one of the lines traced by the read gradient along the second dimension. In essence, the resultant trajectory in *k*-space resembles a zig-zag raster, which eventually covers the desired area.

For example, to create a typical image with  $64 \times 64$  pixels in plane, a frequency-encoding gradient waveform with 64 lobes (32 negative and 32 positive ones, alternatively) needs to be applied, which should happen well within the time of one signal decay. Gradient switching therefore has to happen extremely quickly, and with sufficient stability so that the image does not suffer from artefacts. With typical current technology, it takes approximately 25–40 ms to perform 64 spatial encoding steps (in a classic  $64 \times 64$  acquisition matrix). This limit is determined partly by the physical limits of the scanner and partly by the biological limits of the subject. If the rate of

change and the magnitude of the frequency-encoding gradient field are too high, currents may be induced in the peripheral nerves, creating the sensation of twitching, which is not dangerous but neither is it desirable.

Three methods exist for switching the gradients rapidly.<sup>10</sup> One is to have extremely high-powered gradient amplifiers – a brute force approach. Another is to create gradient waveforms that match the characteristic frequency of the amplifiers and the gradient coils – providing less flexibility in adjusting the gradient readout parameters. A third is to use a low-inductance gradient coil which does not require a large amount of power to create a rapidly switched and strong gradient. For imaging humans, the first systems used for EPI were either the resonant type (e.g. Massachusetts General Hospital NMR Center) or standard clinical systems equipped with home-built low-inductance gradient coils (e.g. Medical College of Wisconsin Biophysics Research Institute). The use of local gradient coils, while cheap, does not offer much room for patients or for stimulus delivery. The introduction of EPI on clinical scanners – using the brute force high-powered gradient amplifier approach – was critical in the explosive growth in fMRI applications. This allowed users to simply buy a system for doing EPI rather than relying on the development of a system by a local team of physicists. Currently, hundreds of such systems are in operation, whereas, in 1992, only a small handful of centers could perform EPI. It should be noted that although EPI is a very fast method, it generally has poorer spatial resolution than conventional MRI techniques. However, the gain obtained in the speed of acquisition is substantial, and without its implementation, the proliferation of fMRI would not have taken place.

### **Pulse sequences**

MRI pulse sequences are the programs that control the timings of the magnetic field gradients, RF pulses, and RF receivers. Essentially, a pulse sequence is a computer program giving a list of instructions to the MRI scanner to control all the elements that go into obtaining an image. For example, one pulse sequence might conceptually be as shown in Figure 1.4, demonstrating the application of the RF pulse (at a 90° flip angle) and the switching on and off of the gradients in three dimensions ( $x$ ,  $y$  and  $z$ ). Note that TE is the time between the RF pulse and the measurement of the signal. This process is repeated 128 times in order to obtain the image and increase detection of the signal.

MR physicists spend some of their time optimizing the parameters of the pulse program to tailor the sequences to the desired application. Different

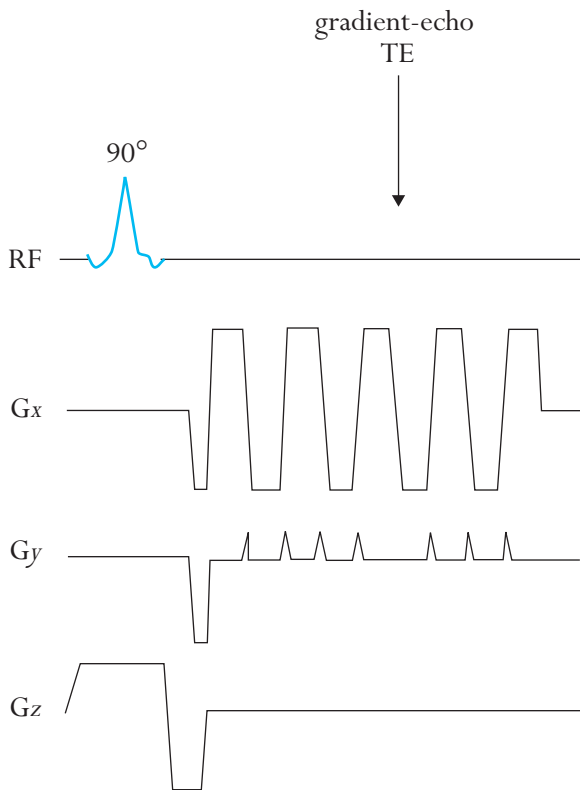


**Figure 1.4** A conceptualization of a typical echo planar imaging (EPI) pulse sequence. TE, Time between the radiofrequency pulse and measurement of the signal.

types of manipulations (e.g. number of gradient switches, length of RF pulse, frequency of RF pulse or the echo time) can alter the signal that is received, and can be used to obtain images with different characteristics (both temporal and spatial). Other modifications of the pulse sequence program may be carried out to alter the contrast of the images in order to address specific neuronal and/or physiologic information (discussed in more detail in *Extracting neuronal and physiologic information*, see later).

### RF receivers and coils

Gradient coils are used to vary the magnitude of the magnetic field gradient in a linear fashion along varying axes. A different type of coil is used to receive the RF signals that are emitted from the protons when excitation ceases. These are the coils that read the incoming signal. Decoding the signal (see earlier) described the nature of the incoming signal and how it is mapped from  $k$ -space to real (subject) space, and transformed into the MR image; this section describes the hardware that is used to collect the signal.

For whole brain imaging, a quadrature 8–12 RF coil is typically used. This coil, which in many systems is brought over the head and face of the subject as they lie in the scanner, is used both to send RF pulses to excite the protons and to receive the incoming signals. Most clinical RF coils are sensitive to signals from the entire head and upper neck area, and are therefore not ideal for fMRI of the brain. This is because they work better when they are tailored to produce a homogeneous RF field over a smaller region of space. Furthermore, the main magnetic field is also more homogeneous over a smaller volume. Gains typically in the range of 30% in the S:N ratio can be obtained by using an RF coil that is closer to the head and has a reception field that does not extend beyond the base of the brain. One should be aware that, again, while a gain of 30% in the S:N ratio is good, the temporal S:N ratio is what really matters in fMRI. At typical voxel volumes ( $3 \times 3 \times 5 \text{ mm}^3$ ), a gain of 30% in the S:N ratio will likely translate to no more than a gain of about 10% in the temporal S:N ratio, given the presence of cardiac and respiratory fluctuations over time.

It is desirable to improve the spatial resolution of fMRI and, hence, smaller and smaller voxel sizes are currently used. This has the advantage of reducing partial volume effects. Furthermore, in voxels that contain gray matter parenchyma, it maximizes the amount of signal change due to functional contrast, since there is less contamination from other tissue types where there is no blood oxygenation-level dependent (BOLD)-related signal change, such as white matter and cerebrospinal fluid (CSF). However, this gain is partly counteracted by a loss in the S:N ratio of each voxel, as the number of protons in the voxel volume decreases. Therefore, at each field strength there is an optimum voxel size that maximizes these two competing mechanisms.<sup>11</sup>

If very high resolution is required over a specific and highly localized region of interest (e.g. the visual or motor cortex), then surface coils can be used. This means that a small RF coil is placed over the region of interest. The S:N ratio in this region is a function of the coil size – the smaller the coil, the greater the S:N ratio. One problem with surface coils, however, is that they do not have a homogeneous reception or excitation field. This is a problem for reception in that the sensitivity drops off rapidly. It is a larger problem for excitation since the excitation energy is inhomogeneously distributed, meaning that in one part of the brain spins receive an excitation of  $90^\circ$  (flip angle) and, in another region, different flip angles might be excited (flip angles are discussed in Resonance and the Larmor frequency, see earlier). To create a homogenous flip angle distribution, it is necessary to use either specialized excitation pulses or a larger coil for excitation. Typically, at 1.5 T, whole body

RF coils are typically used for excitation, therefore obviating this problem. At field strengths  $> 3$  T, whole body coils are not yet feasible. A workable strategy has been to use an intermediate-sized coil for excitation and smaller coils inside the large coil for reception. In this case, a large excitation coil gives a homogeneous distribution of RF power and the surface receiver coil focuses on a specific region for high resolution and/or a high S:N ratio fMRI.

Surface coils can be combined into arrays to increase the S:N ratio and brain coverage. In addition, specific pulse sequences involving RF sensitivity encoding are being designed to make use of independent surface coil arrays to increase the S:N ratio, imaging speed and resolution. Significant advancements in this area are expected in the near future.

### *Extracting neuronal and physiologic information*

Several types of physiologic information can be mapped using fMRI. This information includes baseline cerebral blood volume (CBV),<sup>12, 13</sup> changes in blood volume,<sup>14</sup> baseline and changes in cerebral perfusion,<sup>15-19</sup> and changes in blood oxygenation.<sup>1, 3, 20-24</sup> Recent advances in fMRI pulse sequence and experimental manipulation have allowed quantitative measures of oxygen extraction fraction,<sup>25</sup> cerebral metabolic rate of oxygen (CMRO<sub>2</sub>) changes<sup>26-29</sup> and dynamic non-invasive measures in blood volume<sup>30</sup> with activation. It is beyond the scope of this chapter to review all of these methods. Similarly, the exact mechanisms of the change in blood oxygenation that occur with brain activity are not completely understood, and more detailed discussion on this point can be found in Arthurs and Boniface<sup>31</sup> and Attwell and Iadeola.<sup>32</sup> Below, a brief overview of the role of blood oxygenation in brain function is given, the most common method to obtain activity-related contrast; fMRI relies directly on this parameter. Some advantages and disadvantages of this method are discussed, as is the issue of hemodynamic specificity. Lastly, a particularly interesting emerging method to detect CMRO<sub>2</sub> changes directly will be briefly considered.

#### **Blood oxygenation**

Cerebral blood flow (CBF), and the rate of oxygen consumption by cells, as a result of oxidative phosphorylation, are directly coupled to neuronal activity. Oxygen consumed by neurons is supplied by the blood, where oxygen is bound to hemoglobin. Arteries carry hemoglobin which is fully oxygenated.

<b>Table 1.2 Summary of the practical advantages and disadvantages of pulse sequences that have contrast based on blood oxygenation-level dependent (BOLD), perfusion, volume, and cerebral metabolic rate of oxygen (CMRO<sub>2</sub>) signals</b>		
	<i>Advantages</i>	<i>Disadvantages</i>
BOLD	Highest functional activation contrast by a factor of two to four over perfusion Easiest to implement Multislice trivial Can use very short times between radiofrequency pulses (TR)	Complicated non-quantitative signal No baseline information Susceptibility artifacts
Perfusion	Unique and quantitative information Baseline information Easy control over observed vasculature Non-invasive No susceptibility artifacts	Low functional activation contrast (up to 7 T) Longer TR required Multislice is difficult Slow mapping of baseline information
Volume	Unique information Baseline information Multislice is trivial Rapid mapping of baseline information	Invasive Susceptibility artifacts Requires separate rest and activation runs
CMRO <sub>2</sub>	Unique and quantitative information	Semi-invasive (requires CO <sub>2</sub> inhalation) Low functional activation contrast Susceptibility artifacts Processing intensive Multislice is difficult Longer TR required

When cells are ‘working’ they need to extract this oxygen in the blood supply and, consequently, in the veins, most of the hemoglobin becomes deoxygenated. As early as the 1930s it was known that deoxyhemoglobin was paramagnetic (susceptible to magnetization) and oxyhemoglobin was diamagnetic.<sup>33</sup> In 1982, it was discovered that changes in blood oxygenation changed T2 of blood, but it was not until 1989 that this knowledge was used to image *in vivo* changes in blood oxygenation.<sup>34</sup> The BOLD contrast (a term coined by Ogawa et al<sup>2</sup>) was used to image the activated brain for the first time in 1991. The basic concept behind this endogenous contrast

mechanism is that increases in brain activity are almost invariably accompanied by increases in blood flow. This localized increase in blood flow causes an increase in blood oxygenation which exceeds the metabolic need (i.e. far more oxygen is delivered than is actually required).

Because the supply of oxygen exceeds demand, the excess oxygen is returned by the veins, causing a sudden increase in the amount of oxygenated hemoglobin of the venous return. The original (baseline) levels of deoxyhemoglobin in the blood would normally cause  $T2^*$  and  $T2$  to be decreased. (Remember,  $T2$  is the natural decay of protons precessing in the transverse plane and  $T2^*$  is the same decay within an inhomogeneous magnetic field.) Following the increase in the relative concentration of oxygenated hemoglobin of the venous blood (and the corresponding decrease in the amount of deoxyhemoglobin),  $T2^*$  and  $T2$  increase, leading to a small signal increase in  $T2$ - and  $T2^*$ -weighted images. Although the relative sensitivity of this effect is low (the signal change is of the order of 1–3% at 1.5 T), the advent of rapid imaging techniques such as EPI have simplified its implementation, and BOLD contrast using gradient-echo imaging has emerged as the most commonly used fMRI method.

#### *Advantages in BOLD contrast imaging*

With BOLD contrast, several distinct advantages exist. First, it is, of course, completely non-invasive. Second, the functional contrast to noise is at least a factor of two to four greater than that seen in perfusion or in CBV-based imaging techniques. Third, it is easiest to implement since it only requires, typically, a gradient-echo sequence with an echo time (TE) of 30–40 ms. Fourth, the technique is fast enough to incorporate multi-slice, whole brain echo acquisition. All that is required is that the repetition time (TR) is long enough to accommodate all of the slices in each volume. Typically, with a TE of about 40 ms, the total time for acquiring a single-shot EPI is about 60–100 ms, which translates to a rate of 10–16 slices/s. This is a massive improvement in temporal resolution when compared with other techniques such as positron emission tomography (PET) or single photon emission computed tomography (SPECT). If a reduced number of slices is allowed, then a very short TR can be utilized for fine temporal mapping of the dynamics of the BOLD signal change.

#### *Disadvantages in BOLD contrast imaging*

Several disadvantages exist in regard to BOLD contrast imaging. First, the nature of the BOLD contrast is extremely complicated, involving the interplay

of perfusion,  $CMRO_2$  and blood volume changes, and is modulated by the heterogeneity of the vasculature and neurovascular coupling over time and space. This problem leads to limits of interpretation of the location, magnitude, linearity, and dynamics of the BOLD contrast signal. In addition, it makes across-population comparisons, clinical mapping and pharmacologic-effect mapping extremely challenging. This is because it is assumed that all these parameters hold true across brains and this may not necessarily be the case in the diseased brain. Second, when it comes to pharmacology, it is difficult to establish what effect the medication taken by the clinical populations may be having on CBF, neurovascular coupling, or both. Also, unlike the perfusion and volume mapping methods, no baseline oxygenation information can, as yet, be obtained, since resting state  $T2^*$  and  $T2$  times are dominated by tissue type rather than oxygenation state. However, progress is being made.<sup>35</sup> If resting state oxygenation information is implied, considerable assumptions have to be made regarding blood volume and vessel geometry, among other things. Another problem with BOLD contrast in general is that the same susceptibility weighting that allows for the observation of the functional contrast also contributes to many of the artifacts in the images used. These artifacts include signal dropout at tissue interfaces and at the base of the brain. This dropout occurs because the interfaces of tissues have different magnetic susceptibilities; the protons precess at different frequencies and begin to cancel each other out, and the loss of phase coherence occurs more rapidly. The problem becomes greater at higher field strengths.

### **Hemodynamic specificity**

With the BOLD technique described above, the precise type of observable cerebrovascular information can be more finely delineated. While the information described below is typically more than most fMRI users are primarily concerned with, it is useful to have an abbreviated summary of how specific MRI can be. Please refer to Figure 1.5 for a schematic depiction of pulse sequence sensitization to specific vascular components and the heterogeneity of the vasculature across voxels. It shows intravascular and extravascular signals. If the specific vessel type is filled in (red, arteries; blue, veins), then there exists a contribution from intravascular effects (protons spinning in blood vessels). If the region around the vessel is filled in, then there are extravascular spins (water spins that are in the tissue); extravascular susceptibility gradients contribute to the functional contrast.

Regarding susceptibility contrast imaging, spin-echo sequences are more sensitive to small susceptibility compartments (capillaries and red blood

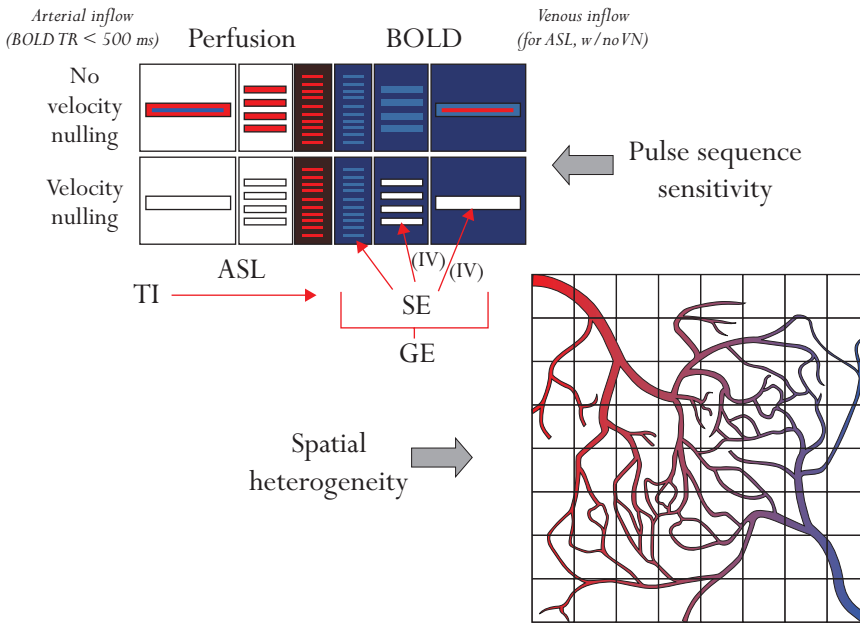


**Figure 1.5** A schematic depiction of pulse sequence sensitization to specific vascular components and the heterogeneity of the vasculature across voxels ASL, Arterial spin labeling; BOLD, blood oxygenation-level dependent; GE, gradient echo; IV, intravascular; SE, spin echo; TI, a time constant; TR, time between successive radiofrequency pulses; VN, velocity nulling.

cells) and gradient-echo sequences are sensitive to susceptibility compartments of all sizes.<sup>36–40</sup> A common mistake is to assume that spin-echo sequences are sensitive to capillaries only. Since red blood cells are also small compartments, spin-echo sequences are selectively sensitive to intravascular signals arising from small and large vessels.<sup>41</sup> Since BOLD contrast is highly weighted by the resting state blood volume that happens to be in the voxel, it is likely that many voxels having pial vessels running through them will have at least 50% blood volume. These voxels are therefore likely to show the largest gradient-echo and spin-echo signal changes. At field strengths approaching 9 T, intravascular spins may no longer contribute since T2\* and T2 of blood becomes extremely short.

Performing BOLD contrast fMRI at high field strengths has the same effect as diffusion weighting in the context of susceptibility-based contrast because T2\* and T2 of venous blood become increasingly shorter than T2\* and T2 of gray matter as field strength increases, therefore less signal will arise from intravascular space at higher field strengths.<sup>4</sup> This unique characteristic of

imaging at high field strengths can be put to use in the creation of high-resolution *venograms* (vein maps of the brain).<sup>4</sup>

### Mapping of CMRO<sub>2</sub> – advances in imaging

Recently, significant advances in mapping activation-induced changes in CMRO<sub>2</sub> using fMRI have emerged.<sup>26,28,29,42</sup> The basis for this method is the realization that the BOLD signal change between two levels of brain activity (baseline and some active state) can be modeled by an expression which combines the effect of the change in CMRO<sub>2</sub> and the change in CBF. The dependence of this BOLD signal change on CBF alone can be mapped by allowing subjects to perform the same task while breathing at least two different concentrations of CO<sub>2</sub> (hypercapnia).

Normalization or calibration using a hypercapnia stress (increasing the CO<sub>2</sub> levels in the air) has evolved to be a method for reducing the number of unknown parameters to allow for mapping of changes in CMRO<sub>2</sub>.<sup>26</sup> The basic concept here is that when the brain is activated, increases in flow, volume and oxygenation are accompanied by an increase in CMRO<sub>2</sub>. When a subject (at rest) is undergoing a hypercapnic stress [5% CO<sub>2</sub>, i.e. the subject is breathing in a gas with a small proportion (1–5%) of CO<sub>2</sub> in it], only the CBF and CBV will change without an accompanying increase in CMRO<sub>2</sub>. Therefore, less oxygen is extracted from the blood, allowing the blood oxygenation change, relative to the perfusion change, to be greater than with brain activation. The change in BOLD signal and the change in blood flow are separately measured at each level of hypercapnia.

If the change in the BOLD signal is plotted versus the measured change in blood flow, curves of constant CMRO<sub>2</sub> are obtained. When subjects performed the desired tasks, the measured changes in the BOLD signal and the CBF generate curves that travel between the iso-CMRO<sub>2</sub> contours. By comparing the ratio of the (simultaneously measured) perfusion and the BOLD signal changes during hypercapnia, and during brain activation, CMRO<sub>2</sub> information can be derived. The information is derived either by fitting the data to the model using the iso-CMRO<sub>2</sub> contours obtained in the first part of the experiment or by numerically interpolating the data.

Methods for extraction of baseline CMRO<sub>2</sub> are on the immediate horizon.<sup>43</sup> The key to these techniques is the more precise extraction of hemodynamic information, such as blood volume and blood oxygenation, and the use of appropriate calibration procedures.

CMRO<sub>2</sub> change mapping is still a work in progress. Its big potential is that the information is unique and perhaps most associated with neuronal

activity. Of course, to derive this information, several still-unresolved assumptions about the hemodynamic changes with CO<sub>2</sub> stress, and about the perfusion and BOLD signal itself, have to be made. Since this method for mapping CMRO<sub>2</sub> changes uses techniques that simultaneously map perfusion and BOLD signals, it has all of the disadvantages of both techniques, and at least one more. The additional disadvantage is that it typically requires the subject to breathe a gas mixture of elevated CO<sub>2</sub> for at least 2 min. This is slightly uncomfortable for the motivated volunteer and may even be lethal to a patient. However, the data collected so far shows excellent agreement with data collected by alternative means. Furthermore, the models employed so far appear to be very robust and relatively insensitive to variations in the value of the empirical constants employed in the model.

### *Advancements in understanding the blood oxygenation-level-dependent (BOLD) signal*

For many users, the issues involved in determining the precise neural underpinnings of BOLD contrast may seem an esoteric after > 10 years of successful implementation of fMRI. It is clear that changes in BOLD contrast-derived maps, for the most part, correlate well with maps derived using other techniques. BOLD is successful for these reasons. While the success of BOLD contrast has, of course, allowed new insights into human brain function to be derived, the technique can certainly have much more potential in regard to spatially resolved quantification of neuronal activity. We, as users, would love to use it for ever more applications: for more precise comparison of subject populations, parametric manipulations, and extraction of transient neuronal activity; for better understanding networked activity; for understanding coupling variations in disease and healthy subjects, and for deriving maps of resting state activity.

In this section, the specific characteristics, including location, latency, magnitude, and linearity of the fMRI signal, will be described in more detail. Emphasis will be placed on how this understanding relates to practical implementation of fMRI.

#### **Location**

In the resting state, hemoglobin oxygen saturation is about 95% in arteries and 60% in veins. The increase in hemoglobin saturation with activation is

largest in veins, changing in saturation from about 60–90%. Likewise, capillary blood changes from about 80–90% saturation. Arterial blood, already near saturation, shows no change.

The second reason why the strongest BOLD effect is seen in draining veins is that activation-induced BOLD contrast is highly weighted by blood volume in each voxel. Since capillaries are much smaller than a typical imaging voxel, most voxels, regardless of size, will likely contain about 2–4% capillary blood volume. In contrast, since the size and spacing of draining veins is on the same scale as most imaging voxels, it is likely that veins dominate the relative blood volume in any voxel that they pass through. Voxels that pial veins pass through can have 100% blood volume, while voxels that contain no pial veins may have only 2% blood volume. This stratification in blood volume distribution strongly determines the magnitude of the BOLD signal.

As illustrated in Figure 1.5, different RF pulse-sequence weightings can give different locations of activation. For instance, in regard to imaging perfusion and BOLD contrast, while much overlap is seen, the hot spots vary by as much as 10 mm. The perfusion change map is sensitive primarily to *capillary* perfusion changes, while the BOLD contrast activation map is weighted mostly by *veins*. A potential worry regarding fMRI location is that venous blood, flowing away from the activated area, may maintain its elevated oxygen saturation as far as 1 cm away. When observing brain activation on the scale of centimeters, this has not been of major concern; however, with increased spatial resolution this will likely become an important issue.

## Latency

One of the first observations made regarding fMRI signal changes is that, after activation, the BOLD signal takes about 2–3 s to begin to deviate from baseline.<sup>23,44</sup> This is often referred to as the hemodynamic delay. This can be seen in the right-hand panel of Figure 1.2, where approximately 2 s elapse after stimulus presentation (at time 0) prior to an increase in the MRI signal. Since the BOLD signal is highly weighted towards venous oxygenation changes, with a flow increase, the time for venous oxygenation to start to increase will be about the time that it takes blood to travel from arteries to capillaries and draining veins – 2–3 s. The hemodynamic impulse response function has been effectively used to characterize much of the BOLD signal change dynamics<sup>45–47</sup> and has been derived empirically by delivering very brief and well-controlled stimuli. Additionally, it can be derived by deconvolving the stimulus input from the measured hemodynamic response.<sup>48,49</sup>

This type of analysis assumes that the BOLD response behaves in a manner that can be completely described by linear systems analysis, which is still an open issue.

If task onset or duration is modulated, the accuracy with which one can correlate the modulated input parameters (stimuli) to the measured output signal depends on the variability of the signal within a voxel or region of interest. In a study by Savoy et al,<sup>50</sup> addressing this issue, variability of several temporal sections of a stimulus-induced response were determined. Six subjects were studied and, for each subject, 10 activation-induced response curves were analyzed. The relative onsets were determined by finding the latency with which the correlation coefficient was maximized with each of three reference functions, representing three parts of the response curve – the entire curve, the rising section, and the falling section. The standard deviation (SD) of the whole curve, rising phase, and falling phase were found to be 650, 1250, and 450 ms, respectively.<sup>51</sup> Across-region differences in the onset and return to baseline of the BOLD signal during primary visual activation<sup>52</sup> and cognitive tasks have been observed.<sup>53</sup> For example, during a visually presented, event-related, word-stem completion task, Buckner et al<sup>53</sup> reported that the signal in the visual cortex increased about 1 s before the signal in the left anterior prefrontal cortex. One might argue that this observation makes sense from a cognitive perspective, since the subject first observes the word stem then, after about 1 s, generates a word to complete this task. Others would argue that the neuronal onset latencies should not be  $> 200$  ms. Can inferences of the cascade of brain activation be made on this timescale from fMRI data? Without a method to constrain, or work around, the intrinsic variability of the onset of the BOLD signal over space, such inferences should not be made in temporal latency differences  $< 4$  s. Combined techniques, such as fMRI with electroencephalography (EEG), are currently under development to address these issues.

Lee et al<sup>54</sup> were the first to observe that the fMRI signal change onset within the visual cortex during simple visual stimulation varied from 6 to 12 s. These latencies were also shown to correlate with the underlying vascular structure. The earliest onset of the signal change appeared to be in gray matter and the latest onset appeared to occur in the largest draining veins. Similar latency dispersions in the motor cortex have been observed. In one study, latency differences, detected in the visual cortex using the Hilbert transform, did not show a clear correlation of latency with evidence for draining veins.<sup>55</sup>

## Magnitude

The magnitude of the fMRI signal change is influenced by variables which can vary across subjects, neuronal systems, and voxels.<sup>39</sup> To make a complete and direct correlation between neuronal activity and the fMRI signal change magnitude, in a single experiment, all the variables which influence these changes must be characterized on a voxel-wise basis. Because of these primarily physiologic variables, brain activation maps typically show a range of BOLD signal change with magnitudes of 1–5% (at 1.5 T, GE sequence, TE = 40 ms), and higher with greater field strengths (up to 15% at 4 T). In the past several years, considerable progress has been made in characterizing the magnitude of the fMRI signal change with underlying neuronal activity. Figure 1.6 shows a flow chart roughly outlining both the complicating factors behind the fMRI signal as well as the richness of information contained within it.

First, it was clear that areas that showed significant BOLD signal change were in the appropriate neuronal area corresponding to specific well-characterized tasks. Second, inferred neuronal modulation was carried out by systematically varying some aspect of the task. Clear correlations

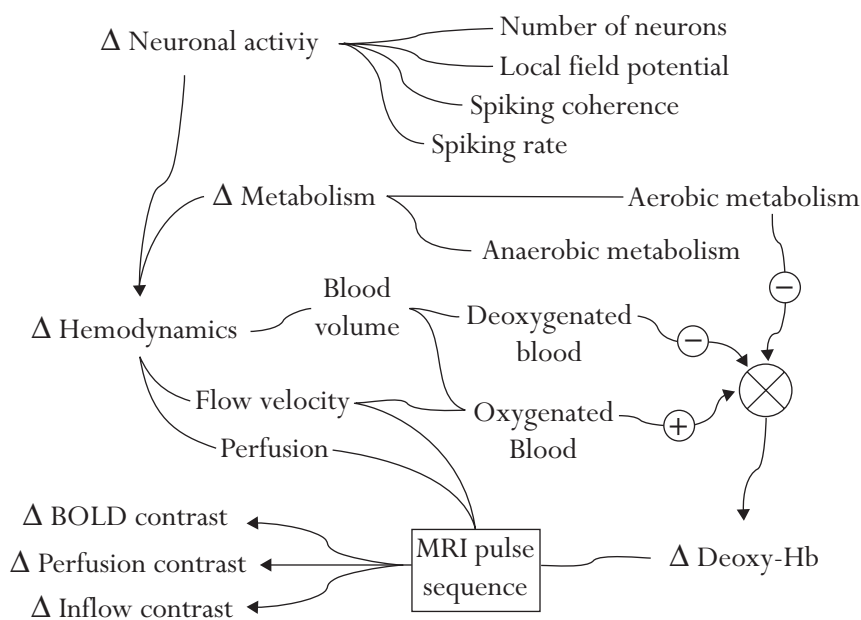


**Figure 1.6** Flow chart outlining both the complicating factors behind the functional magnetic resonance imaging (fMRI) signal as well as the richness of information contained within it.

between BOLD signal change magnitude and visual flicker rate, contrast, word presentation rate, and finger-tapping rate were observed.<sup>3,56–58</sup>

Recently, several studies have emerged correlating measured neuronal firing rate with well-known stimuli in animals<sup>59</sup> and humans,<sup>60,61</sup> demonstrating a high correlation between BOLD signal change and electrophysiological measures. A recent article by Logothetis et al<sup>62</sup> described the simultaneous measurement of electrical activity and BOLD contrast in primate visual cortex, and revealed a linear relationship between neuronal activity and stimuli contrast, albeit with one caveat – the lower the level of neuronal activity, the more BOLD contrast overestimated the degree of neuronal activity. In other words, BOLD contrast does indeed change in proportion to the degree of neuronal activity, but the relative rate at which it changes with neuronal activity is generally less. Results from this article have not only impacted how fMRI signal changes are interpreted in terms of magnitude of change with a change in a task but have also shed light on some issues regarding the dynamics of fMRI contrast, as described below.

### Linearity

Understanding the relationship between fMRI signal change magnitude and neuronal firing rate is critically important for both the clearer interpretation of experimental results and also for experimental design. Described above was the relationship between BOLD signal change magnitude and neuronal activity at a steady state, or after several seconds of continuous activity. Described in this section is the relationship between BOLD contrast and neuronal activity over time during very brief neuronal stimulation. Does the BOLD signal change increase in a manner that is directly linear with stimulus duration? It has been found that, with very brief stimulus durations, the BOLD response shows a larger signal change magnitude than expected from a linear system.<sup>63,64</sup> This greater than expected BOLD signal change is generally specific to stimuli durations < 3 s. Reasons for a greater than expected event-related response may be neuronal, hemodynamic, and/or metabolic in nature. The neuronal input may not be a simple boxcar function. Instead, an increased neuronal firing rate at the onset of stimulation (neuronal ‘bursting’) may cause a slightly larger amount of vasodilatation that later plateaus at a lower steady state level. Results from Logothetis et al<sup>62</sup> have demonstrated clearly this ‘bursting’ at the onset of visual stimulation. In the visual cortex, this effect has been extremely well characterized in past literature describing single unit recordings.

BOLD contrast is highly sensitive to the interplay of blood flow, blood volume, and oxidative metabolic rate. If, with activation, any one of these variables changes with a different time constant, the fMRI signal may show fluctuations until a steady state is reached.<sup>65,66</sup>

It is clear that, in spite of the widespread use of fMRI and the success that the method has had in the study of brain function, there are still a lot of unanswered questions about the specific manner in which physiological, metabolic, and vascular aspects interact in response to increased neuronal activity, and how they manifest themselves in the BOLD response. However, the elucidation of these questions constitutes one of the most interesting aspects of this field, and current investigations are encouraging.

---

### *Positron emission tomography (PET) and single photon emission computed tomography (SPECT)*

---

Since Langley's (1878) hypothesis of 'receptive substances' involved in the response to pharmacological agents, much work has been done to reach the current concept of neuroreceptors.<sup>67</sup> They consist of large protein or glycoprotein molecules commonly located on the cell surface, which are responsible for mediating the action of both endogenous neurotransmitters and exogenous pharmacologic agents in the nervous system. Several neurotransmitters and respective receptors have been characterized and implicated in brain physiology.

Using radioactive-labeled ligands and autoradiographic techniques, it is possible to visualize the distribution of several kinds of neuroreceptors *in vitro* and *ex vivo*. The same principles have now been applied to allow the visualization and measurement of neuroreceptors *in vivo*. PET and SPECT provide a unique means to investigate neurochemical abnormalities in neuropsychiatric conditions, as well as to study the mechanisms of action of drugs.<sup>68</sup> This section will briefly review some basic aspects of PET and SPECT neuroreceptor imaging as a basis for understanding data presented in the following chapters of this book.

#### **Basic principles of PET and SPECT**

Emission tomography techniques are based on the *in vivo* administration of radioisotope-labeled tracers or ligands (radiotracer/radioligand) with affinity for the target structures (e.g. neuroreceptors and enzymes). The

radioisotopes are unstable (proton-rich nuclides) and decay to a more stable state emitting gamma ( $\gamma$ ) rays in the process. PET or SPECT cameras are able to detect the emitted  $\gamma$ -rays and provide a tomographic image of the distribution of the tracer in different regions of the body.

PET tracers are labeled with radioisotopes such as  $^{11}\text{C}$ ,  $^{18}\text{F}$  and  $^{76}\text{Br}$ , that emit positrons ( $\beta^+$  particles), which, after travelling a short distance in tissue, collide with surrounding electrons to form a positronium.<sup>69</sup> Almost instantaneously, the positronium annihilates, forming two photons ( $\gamma$ -rays) of 511 keV, which are released in opposite directions at  $180^\circ$  (Figure 1.7a). Detection of the photons is based on the trajectory and the timing of impact on the camera's detector. The photons are detected or counted if both hit the detector (so-called coincidence detection).<sup>69</sup> The  $180^\circ$  geometry permits good accuracy for localizing the source of the energy along a straight line.

SPECT radiotracers are labeled with photon-emitter isotopes such as  $^{123}\text{I}$  and technetium-99m (Tc-99m). Photon-emitter isotopes have unstable nuclei due to a deficiency in the number of neutrons and may, as an alternative to positron emission, capture an orbiting electron into the nuclei.<sup>70</sup> The captured electron transforms a proton into a neutron, emitting a cluster of photons ( $\gamma$ -ray) in the process. Emissions of photons occur randomly and in  $360^\circ$  geometry (Figure 1.7b). Each emitted photon is singular and independent in

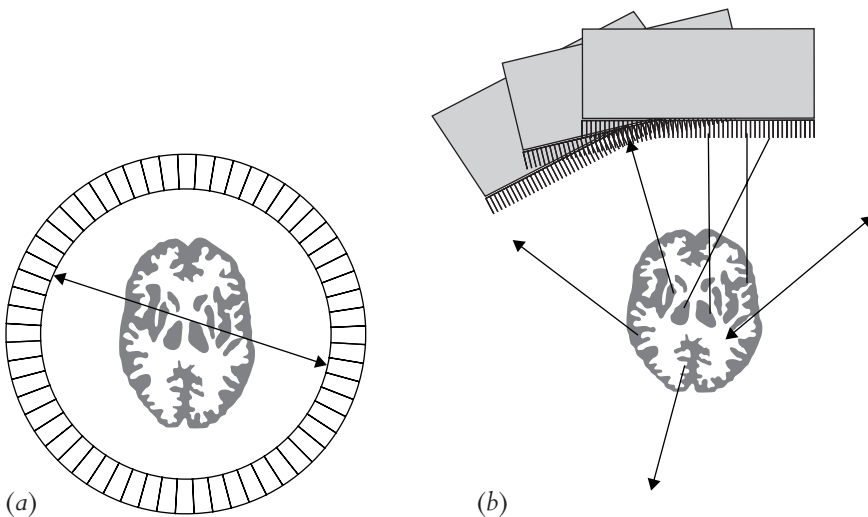


**Figure 1.7** (a) Positron emission tomography (PET) (adapted from Meikle and Dahlbom<sup>69</sup>); (b) single photon emission computed tomography (SPECT) (adapted from Distance Assisted Training Program for Nuclear Medicine Technologists, 2000, <http://casino.cchs.usyd.edu.au/mrs/iaea/>)

nature, hence single photon.<sup>71,72</sup> In brain SPECT the detectors rotate around the subject's head and the data are acquired over 360°.

PET and SPECT gamma cameras detect the emitted  $\gamma$ -rays when they hit crystals in the surrounding detectors. The light energy generated in the crystals is converted to an amplified electrical pulse through the photomultiplier tubes, which allows the computer to map different intensities of energy onto a frequency map in three dimensions, where energy is characterized according to intensity with a pulse height analyzer.<sup>73</sup>

SPECT cameras use collimators (lead sheets with thin holes) to prevent photons outside the line of a particular plane from impacting on the detectors (Figure 1.5b). Any photon that reaches the detector is assumed to originate from a particular plane in the subject directly beneath and parallel to the holes in the collimator. Although collimators are crucial for SPECT imaging, they are also the limiting factor for sensitivity (number of photons that pass through the collimator) and resolution (number of photons excluded to minimize detection of scatter and attenuated photons).<sup>71</sup>

PET imaging has generally higher sensitivity and resolution due to the 180° coincidence event, which eliminates the need for physical collimation. Problems such as scatter ( $\gamma$ -rays impacting on the detector away from their line of trajectory) and attenuation ( $\gamma$ -rays slowed by progress through the tissues) are minimized in PET. However, new SPECT cameras and computational methods for scatter and attenuation correction have significantly improved the quality of SPECT images, narrowing the gap with PET imaging.<sup>74</sup>

## Radioligands

In order to provide accurate binding estimates the radioligands need to fulfil several criteria.<sup>75</sup> High affinity (nM range) and high selectivity for the target receptor are essential. Minimal lipophilicity is necessary to allow easy and rapid crossing of the blood–brain barrier, but high lipophilicity is not desirable since it is associated with high non-specific binding. Insignificant metabolism is desirable, such that labeled metabolites do not cross the blood–brain barrier to interact with the target binding site during data acquisition. Lack of pharmacological effect at tracer doses (< 100 pmol) and safety for intravenous (IV) injection is necessary. Finally, the labeling process has to be amenable so that the scans can proceed within the time constraints of the radioisotope's half-life.<sup>68</sup>

The development of radioligands that match the above requisites is not an easy process. Radioligands are the limiting factor in the investigation of

neuroreceptor systems. There are PET and SPECT tracers for some receptor systems, such as dopamine (D1, D2, and dopamine transporter), serotonin [(5-hydroxytryptamine) 5HT<sub>1A</sub>, 5HT<sub>2A</sub>, and serotonin transporter], gamma-aminobutyric acid [(GABA) GABA<sub>A</sub>], opiate, cholinergic (muscarinic and nicotinic) and for the enzyme amino acid decarboxylase (AADC).<sup>76</sup> Many interesting targets are lacking appropriate radioligands for *in vivo* investigation. Work is in progress towards developing suitable radioligands for neurotransmitter systems that are highly relevant for neuropsychiatric disorders, but hitherto have not been investigated *in vivo*, such as the glutamatergic system [*N*-methyl-D-aspartate (NMDA), AMPA, kainate and metabotropic receptors].

### Data acquisition

Dynamic imaging protocols are currently preferred to obtain PET and SPECT receptor binding data. These involve the acquisition of sequential images of the same regions over time after radioligand administration. The region-of-interest (ROI) approach is the most commonly employed for analysing receptor images. Regions of interest are defined around brain areas of interest, and regional measures of radioligand uptake obtained in different moments. This process allows the generation of radiotracer uptake and washout.

### *In vivo* neuroreceptor quantification

#### *Basic principles*

The principles of *in vivo* neuroreceptor imaging are based on *in vitro* receptor pharmacology, with the advantage that they investigate functional receptors in living brains, preserving the receptor's natural environment.

The outcome measures most commonly used in *in vitro* pharmacology are the equilibrium dissociation constant ( $K_D$ ) and the receptor density ( $B_{\max}$ ).<sup>77</sup>  $K_D$  is the ratio of the rate of association constant ( $K_{\text{on}}$ ) and the rate of dissociation constant ( $K_{\text{off}}$ ) at equilibrium.  $K_D$  describes inverse binding affinity of the ligand for a determined receptor (the lower  $K_D$  the greater the binding affinity).  $B_{\max}$  is the density of receptors (receptor number per tissue volume) and corresponds to the ligand concentration specifically bound to the receptor at saturation point.

*In vitro* receptor pharmacology is not easily applied to neuroreceptor imaging. The general principle underlying neuroreceptor imaging is that the regional uptake of the radiotracer will be related to the number of receptors for which the tracer exhibits selective affinity.<sup>78</sup> Unlike *in vitro* studies where radioligand concentration is tightly controlled, many variables determine radioligand availability *in vivo*, including: (1) blood–brain barrier permeability;

(2) non-specific binding in the brain; (3) regional CBF (rCBF); (4) rate of peripheral clearance; (5) binding to plasma proteins; (6) potential penetration of radiolabeled metabolites; (7) concentration of endogenous competitor; and (8) partial voluming and cross-scattering from adjacent brain regions.<sup>78,79</sup> These variables have to be taken into account otherwise binding parameters may only remotely relate to the receptor concentration.

The methods to evaluate receptor parameters *in vivo* with SPECT and PET can be divided in two, *quantitative* and *semiquantitative*. The most commonly used outcome measures are the binding potential (*BP*) and the total volume of distribution ( $V_T$ ). *BP* is the total number of receptors multiplied by their affinity for the radioligand ( $BP = B_{\max}/K_D$ ).  $V_T$ , which is defined as the equilibrium ratio of the total concentration of tracer in tissue to the total concentration of parent tracer in plasma.  $V_T$  represents the volume of tracer from the plasma that is extracted by the tissue, thus it expressed in mL plasma/mL tissue. This is a robust parameter, for reversible kinetics, proportional to the specific binding in a brain region and independent of blood flow.

#### *Semiquantitative methods*

Among the semiquantitative methods, the *ratio method* is the most commonly used, calculated by the formula:  $BP' = (R_R - R_T)/R_R$ , where  $R_T$  (target region) is the concentration of activity in the brain regions that are rich in receptors and  $R_R$  (reference region) is the concentration of activity in the brain area devoid of receptors.  $R_T$  and  $R_R$  are defined based on receptor concentrations from post-mortem autoradiography studies. The activity in the target region represents non-specific uptake plus free ligand ( $C_{NS}$ ) and specific binding ( $C_S$ ), whereas in the reference region it represents only  $C_{NS}$  (Figure 1.6). The reference region is used to subtract  $C_{NS}$  of the target region in order to measure  $C_S$ . This ratio method provides an approximation to the saturable component of binding ( $BP'$ ), and is therefore linearly proportional to  $B_{\max}$  when calculated at equilibrium. There are problems in determining equilibrium in these studies, and the ability of semiquantitative methods to provide an accurate value for *BP* needs to be validated by model-based methods.<sup>79</sup>

#### *Quantitative methods*

Model-based methods were developed to provide *in vivo* quantitative estimates of receptor number and affinity. These methods can be divided into *kinetic modeling* and *equilibrium methods*. The *BP* value calculated with quantitative methods incorporates measurements of local radioactivity in the brain tissue and the radioligand input to the brain (arterial concentration) as a

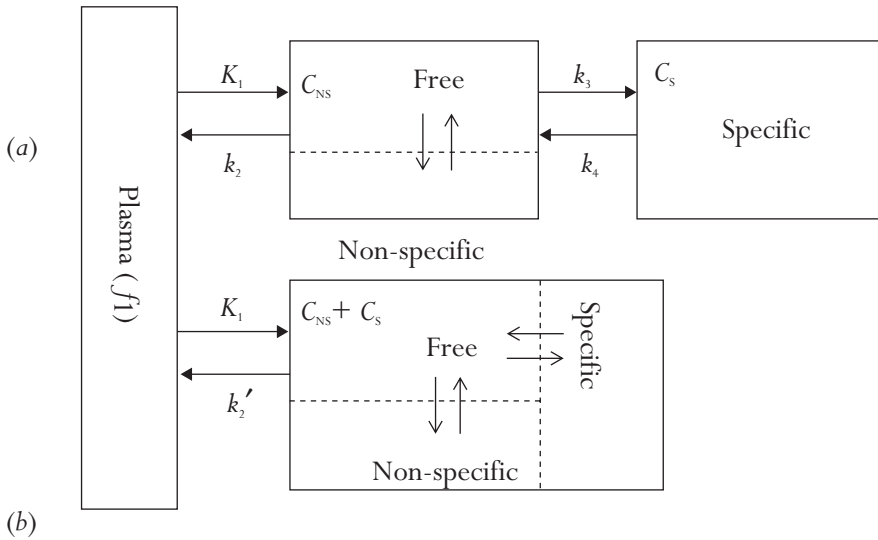


**Figure 1.8** Compartment models. (a) Graphic representation of the two-tissue compartment model (2-TC), where the plasma compartment is the input function and  $f_1$  is the free fraction of the tracer. The  $C_{NS}$  compartment represents non-specific and free tracer, and the  $C_S$  compartment represents specific binding. (b) Graphic representation of the one-tissue compartment model (1-TC), which has the same input function from the plasma compartment, but  $C_{NS}$  and  $C_S$  are combined in one compartment.

function of time.<sup>79</sup> Mintun et al<sup>77</sup> introduced a compartmental *kinetic model* to measure neuroreceptor ligand binding, in which mathematical models try to characterize the kinetics of the radiotracer between plasma, brain and receptor compartments by estimating the rate constants ( $K$ ) (Figure 1.8).

Two compartmental models are commonly described – a two-tissue compartment model (2-TC model; Figure 1.8a) and a one-tissue compartment model (1-TC model; Figure 1.8b). The 2-TC model assumes that the free and non-specifically bound compartments equilibrate rapidly and may then be considered as a single compartment yielding the following parameterization:  $K_1$  (plasma to tissue influx constant),  $k_2$  (tissue to plasma efflux constant),  $k_3 = f_2 k_{on} B_A$  ( $k_3'$  pseudo first-order association rate constant,  $f_2$  is the tissue-free fraction of the tracer,  $k_{on}$  is the first-order bimolecular association rate constant and  $B_A$  is the concentration of available binding sites);  $k_4 = k_{off}$  (disassociation rate constant). The 1-TC model assumes that the free, non-specifically bound and specifically bound compartments all equilibrate rapidly, and may then be considered as a single compartment yielding the following parameterization;  $K_1$  (plasma to tissue influx constant) and  $k_2'$

[tissue to plasma efflux constant:  $k_2' = k_2 / (1 + k_3/k_4)$ ]. The compartmental model estimates  $BP$  using the rate constants obtained in the compartmental analysis, where  $BP = K_1 k_3 / k_2 k_4 f_1$  ( $f_1$  is the plasma-free fraction of the tracer). Quantitative estimation of  $BP$  has been widely used in PET, and has been successfully incorporated to SPECT studies.<sup>80,81</sup> Different model-based methods using on this formulation have been validated to estimate binding parameters including *kinetic analysis*,<sup>77</sup> *graphic models*,<sup>82</sup> and the *reference tissue model*.<sup>83</sup>

The *equilibrium method* is a model-based analysis performed when radioligand distribution is at equilibrium, i.e. when receptor–ligand association and dissociation rates are equal.<sup>80,84,85</sup> Equilibrium is obtained through a bolus plus constant infusion of the radioligand. This paradigm simplifies receptor quantification. It allows the estimation of  $V_T$ , defined as the ratio at true equilibrium of total tissue concentration to a reference concentration (e.g. free metabolite-corrected plasma concentration).  $BP$  is calculated using the ratio of  $V_T$  measurements from regions with specific and non-specific uptake, under the assumption of uniform non-specific binding.<sup>86</sup> Equilibrium studies with constant infusion and can provide a stable baseline for pharmacological challenge experiments.<sup>87</sup>

### Specific technical issues

Many factors can influence the quality of receptor imaging data, e.g. the specific sensitivity of the PET and SPECT cameras, accurate and reliable delineation of ROI, duration of the scan, patient motion between scans, and general suitability of analytical imaging techniques. Careful procedures should be implemented to address these problems, such as the use of fiducial markers (i.e. little sticks containing a tiny bit of radiation that are placed on the subjects head), which help in improving post-acquisition data realignment; head fixation with masks; anatomically guided ROI analysis, ideally guided by a structural MRI of the same subject or via spatial normalization to standard templates; and use of validated model-based analysis.

A major advantage of these radiotracer techniques is extraordinary high sensitivity (about  $10^{-9}$ – $10^{-12}$  M), many orders of magnitude greater than the sensitivities available with MRI (about  $10^{-4}$  M) or MR spectroscopy (about  $10^{-3}$ – $10^{-5}$  M).<sup>68</sup> In terms of spatial resolution, the gap between PET and SPECT has been narrowing. Given ideal imaging conditions, 4–5 mm full width at half maximum (FWHM) is achievable with PET while 8–10 mm FWHM is achievable with SPECT.<sup>3</sup> Progress has recently been made with animal-dedicated PET devices achieving resolutions of about 1–2 mm.

Emission tomography scans implicate exposure to ionizing radiation, which restricts its use under some conditions. Exposition to radiation is a potential risk for the fetus, so pregnancy has to be checked before each scan. Previous exposition to ionizing radiation can be a contraindication to scans. The number of research scans that can be conducted in 1 year is generally limited to two, sometimes four. This is a potential problem for longitudinal studies, such as follow-up studies evaluating the effects of treatment on neuroreceptors. Studies evaluating acute pharmacological challenges can either be performed in a two-scan protocol (baseline and challenge), or in a one-scan protocol using bolus plus constant infusion of the radiotracer. Each radiotracer allows the investigation of one receptor system, and exposure to radiation limits the receptor systems that can be checked in the same subject. Although emission tomography techniques have molecular sensitivity, the number of conditions that can be tested in each study is infinitely inferior to fMRI studies.

## *Methodology*

The preceding sections have provided an introduction to the principles behind the information contained in the MR signal. A description of how and what is acquired with PET and SPECT has also been provided. The hardware used to acquire and process the signal, and some advances in these systems, have also been described.

A further aspect in the understanding of functional neuroimaging is the methodology used by the researcher. Methodology is defined here as the strategies by which the technology and the understanding of the signal are brought to bear on specific applications. While this definition can be quite broad, covering everything including subject handling, subject interface, data processing, and data pooling, the focus in this section is primarily concerned with how neuronal activation paradigms can be designed. A schematic summary of these strategies is shown in Figure 1.9. A description of each of these is given below.

### **Block design**

Block design paradigms are the classical paradigm used in fMRI and are widely reported in the current literature. Essentially adapted from PET paradigm designs, a block design requires a subject to perform a task for

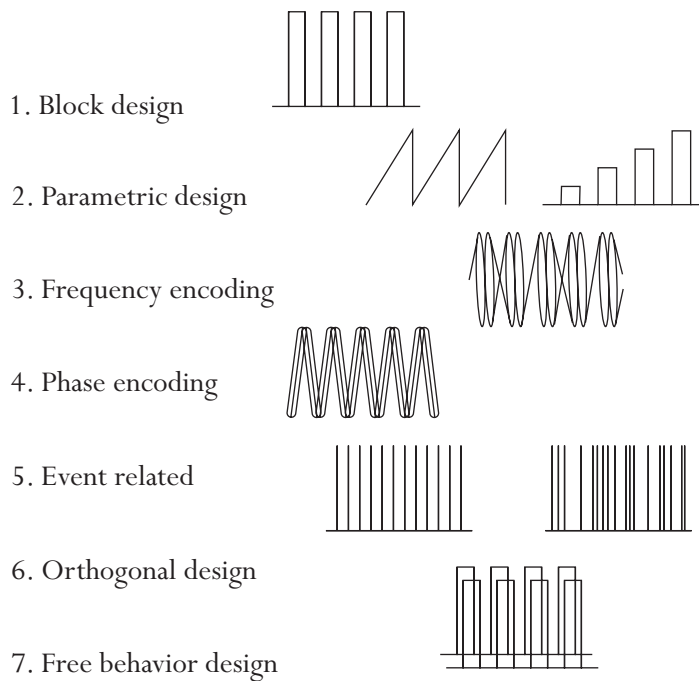


**Figure 1.9** Various neuronal input strategies.

at least 10 s (to reach a hemodynamically steady state), alternated for a similar amount of time with one (AB) or multiple (ABC or ABCD, for example) control tasks. The control task might be something as simple as a fixation cross or more complex. The central tenet of this method is that experimental condition A contains identical cognitive elements to control task B with the addition of the cognitive process of interest. For example, in a study looking at the perception of fear in facial expressions, one control condition might be a face expressing no emotion (neutral) or a different emotion (happy), which would be contrasted with the experimental condition, i.e. a face expressing fear. In this example, all the elements of the experimental condition are also in the control condition (attending to and processing a complex facial stimulus), and only the experimental condition contains what is of interest, i.e. the element of fear. Within each block it is advisable to present your stimulus as many times as possible as it is thought that an increase in the S:R ratio can be obtained with repeated presentation. The drawback of this design is that it is based on a model of pure insertion,<sup>88</sup> which assumes that there are no interactions between the cognitive components of the two conditions.

This may be a useful way of conceptualizing cognitive processes at a behavioral level but neuroimaging investigations suggest that the brain is a highly non-linear system and thus the pure insertion model may not necessarily be appropriate.

There are several reasons to use a block design paradigm. There is an increased S:R ratio over multiple presentations of the stimulus, analysis and interpretation are relatively simple, and it is a useful technique for measuring a physiological state that is sustained over a fairly long (about 1–2 min) period. There are also, however, some limitations which should be borne in mind at the design stage. There may be potential confounds from maintaining attentional and cognitive set, e.g. boredom, reduced attention, habituation or fatigue. This type of design may not be suitable for questions pertaining to cognitive processes that operate on a very short time-scale. Lastly, it is not possible to randomize the presentation of items within each block, although counterbalancing presentation across subjects can, to a certain degree, overcome this problem.

### Parametric designs

Parametric designs make the assumption that neuronal activity is a function of stimulus strength or intensity. It was observed that the fMRI signal increases with the level of intensity of the stimulus and therefore by varying the intensity of the stimulus it is possible to characterize how the brain responds to these changes.<sup>3,56,57</sup> The essential aspect of parametrically designed experiments is that the task itself is varied in some systematic fashion and the corresponding changes in the brain are compared, rather than simply the magnitudes themselves against a single control task. Taking the example from above (see Block design section above), one might compare faces displaying 50 or 100% expressions of fear. The results from tasks such as these are more directly interpretable in that if only two conditions are compared (as in a block design). When the task is systematically varied (as with parametric designs), and the slopes compared on a voxel-wise basis, the spatial variations in blood volume and other physiologic factors not related to brain activation are controlled to some degree. Parametric designs can involve continuous variation of the stimuli or can be set up in a blocked fashion, with each block involving a different degree or intensity of stimulation. As an example of the latter, taking the fearful faces experiment as an example, you might have one block of neutral faces, a second block of mildly fearful faces (50%) and a third block of prototypically (100%) fearful faces.

## Frequency encoding

Frequency encoding is probably the least common of task designs but perhaps lends itself optimally to very specific types of stimuli. The method involves designating a specific on–off frequency for each type of stimulus used. Using Fourier analysis to analyze the data reveals the maximum power under a specific spectral peak corresponding to the brain area specific to the particular on–off frequency. The utility of this method has been demonstrated in the mapping of left and right motor cortex by cueing the subject to perform a finger-tapping task at different on–off rates for each hand.<sup>89,90</sup> In general, the goal of any paradigm design is to encode as much information as possible into a single time series. This allows more precise comparisons since a primary source of error is variation across time series due to scanner instabilities or subject movement. Keeping as many comparisons as possible in one time series is one method to reduce the effects of these variations.

## Phase encoding

Phase encoding the stimulus input involves varying some aspect of the stimuli in a continuous and cyclic manner. This strategy has been most successfully used in performing retinotopic mapping.<sup>91–93</sup> In this type of study, a visual stimulus ring is continuously varied in eccentricity then, after the most extreme eccentricity is reached, the cycle is repeated again. The data are then typically analyzed using Fourier analysis, mapping out the areas that show a signal change temporal phase that correlates with the stimulus phase. This is a powerful technique since it makes use of the entire time series in that there are no ‘off’ states. This method also lends itself to Fourier analysis, and has also been used for somatotopic<sup>94</sup>, and tonotopic mapping.<sup>95</sup>

## Event-related designs

Increasingly, researchers are beginning to use event-related designs in fMRI. Before 1995, a critical question in event-related fMRI was whether a transient cognitive activation could elicit a significant and usable fMRI signal change. In 1996, Buckner et al<sup>53</sup> demonstrated that, in fact, event-related fMRI lent itself quite well to cognitive neuroscience questions. In their study, a word-stem completion task was performed using a block-design strategy and an event-related strategy. Robust activation in the regions involved with word generation were observed using both methodologies. The advantages of event-related activation strategies are many:<sup>96</sup> tasks can be better randomized,<sup>97–99</sup> fMRI analysis can be conducted based on

measured behavioral responses to individual trials,<sup>100</sup> and there is the option to incorporate overt responses into a time series (e.g. a verbal response by the subject). Practice and habituation effects can also be minimized.

One disadvantage of event-related designs is the fact that since (as pointed out above) the BOLD signal change is measured from a single stimulus, many more trials have to be repeated to obtain sufficient S:N ratios. Since the responses need to be singularly and unambiguously assigned to each event, the interstimulus time needs to be at least as long as the typical width of the BOLD response curve (8–10 s). Therefore, these experiments need to be very long, and become prohibitively long for certain subject populations such as children and the elderly.

When using a constant interstimulus interval (ISI), such as might be used in a block-design paradigm, the optimal ISI is about 10–12 s. Dale<sup>101</sup> showed that responses to visual stimuli, presented as rapidly as once every 1 s, can be adequately separated using overlap correction methods. Overlap correction methods are only possible if the ISI is varied during the time series. These results appear to demonstrate that the hemodynamic response is sufficiently linear, or at least additive, to apply deconvolution methods to extract overlapping responses. Burock et al<sup>102</sup> has demonstrated that remarkably clean activation maps can be created using an average ISI of 500 ms. Assuming the hemodynamic response is essentially a linear system, there appears to be no obvious minimum ISI when trying to estimate it. Dale<sup>101</sup> suggested that an exponential distribution of ISI, having a mean as short as is psychophysically possible, is optimal for estimation of the individual hemodynamic responses of each stimulus. One rate-limiting factor in stimulus presentation depends on the study being performed. Many cognitive tasks may require a slightly longer average presentation rate. Additionally, it is possible that for very short ISI (e.g. < 50 ms) there may be logistical difficulties in physically presented stimuli at that speed due to slower refresh rates on presentation screens.

Recent studies by Liu et al<sup>103</sup> and Birn et al<sup>104</sup> have helped to determine the optimal timing parameters to use when performing variable ISI event-related studies. It turns out that the optimal design depends on the question being asked. If one is interested in simply making the most robust map of activation, the longer the stimulation duration the better, and the optimal ISI is such that the average ISI is the stimulus duration, resulting in a 50/50 distribution of on versus off time. If one is interested in creating the most accurate estimate of the hemodynamic response, say for comparisons of subtle changes in activation in a predetermined region, then the shorter the task duration the better.

### **Orthogonal designs**

Orthogonal task design is a powerful extension of block-design studies. The basic concept is that if one designs two different task timings that would create BOLD responses that are orthogonal to each other (i.e. their vector product is zero), then these tasks can be performed simultaneously during a single time series collection with no cross-task interference, making comparison much more precise. This technique was first demonstrated by Courtney et al.<sup>105</sup> In their study, six orthogonal tasks were designed into a single time series. This type of design also lends itself to event-related studies. For example, in a study looking at auditory and visual processing simultaneously, the same time series can be used to collect information from both ‘studies’, as they elicit orthogonal BOLD responses (they have no temporal correlation with each other).

### **Free behavior designs**

For many types of cognitive neuroscience questions, it is not possible to precisely constrain the timing or performance of a task. It is necessary then to allow the subject to perform the task ‘freely’ and take a continuous measurement of the performance (e.g. SCR or change in blood pressure), then use this other measurement as a reference function for subsequent time series analysis. Examples of this type of design are emerging. As an example, changes in skin conductance are difficult to predict or control. In a study by Patterson et al,<sup>106</sup> skin conductance was simultaneously recorded during an array of tasks and during a rest period. The skin conductance signal change was then used as a reference function in the fMRI time series analysis. Several cortical and subcortical regions were shown to have signal changes that were highly correlated with the skin conductance changes. Similarly, this type of design has been used successfully to reveal areas of the brain that are active in patients with schizophrenia during hallucinations. McGuire and colleagues<sup>107</sup> asked subjects to indicate with a button press when they were hearing voices throughout the scanning session, and these responses were later used as an input function in the analysis stage.

## *Applications*

---

Over the past decade, applications of fMRI have expanded as the technology, methodology, and interpretation has improved. Two primary areas of

application have included basic research – understanding the organization of the healthy human brain – and clinical research.

Basic research has involved describing, with greater precision and robustness, the functional anatomy of systems in the developing and adult brain, including motor, visual, auditory, tactile, taste, language, attention, emotion, learning, priming, plasticity, and memory.

Clinical research has involved two primary avenues. The first is towards robust daily clinical application. This depends on the creation of a means by which all types of patients can be rapidly and reproducibly scanned for the purposes of presurgical mapping, perfusion assessment or vascular reserve assessment. Using fMRI in the clinic requires the implementation of a method by which immediate feedback is provided to the user to ensure quality control, accurate functional localization, sufficient brain coverage, and implementation of methods by which regions of activation are rapidly registered to useful anatomical landmarks that can then be used as guides in the context of neurosurgical procedures. The second clinical application has been towards understanding the neural correlates of specific neurological and psychiatric disorders. This can include testing the integrity of basic sensory systems in various disorders (such as visual or auditory) up to exploring far more complicated brain responses to particular symptoms (as in a symptom challenge study). Reviews of the current neuroimaging literature for psychiatric disorders are provided in the following chapters. Steady progress is being made towards using fMRI to better understand human brain organization, and on a meaningful temporal and spatial scale. The advantage of being able to scan individuals repeatedly over time has addressed questions of etiology and disease progression. Similarly, particular patterns of brain activity over time can inform particular predictors of response to certain medications.

### **Applications of neuroreceptor imaging**

The main applications of neuroreceptor imaging are to investigate the pathophysiology of neuropsychiatric disorders and to evaluate interactions of pharmacological agents with receptor systems.<sup>67</sup> In the pathophysiology of neuropsychiatric conditions, these techniques can investigate issues such as regional abnormalities of receptor density, correlations between receptor-binding parameters and clinical variables, neurotransmitter concentrations, and response to pharmacological challenges. In psychopharmacology, these techniques are useful to investigate the receptor-binding profile of drugs, potency of psychotropic drugs (displacement studies), the

dose–receptor-occupancy relationship, receptor occupancy and outcome variables, clinical efficacy and side effects, and in therapeutic drug development (radiolabeling of the drugs allows determination of blood–brain barrier penetration, brain distribution, receptor binding and dosing).

The future possibilities of radiotracer imaging are broad and exciting, going beyond neuroreceptors to include transporters, enzymes, signal transduction and gene expression. For this broader perspective, PET and SPECT methodologies have been described as ‘*in vivo* molecular imaging’, which promises to help answer new scientific questions.<sup>68</sup>

## Conclusions

The aim of this chapter was to provide the reader with a brief overview of the principles of MRI, PET and SPECT. Furthermore, it is hoped that some understanding of the hardware used in the neuroimaging environment has been obtained, along with insight into how these technologies are developing in order to better address specific research questions. The goal was that the reader come away with a better perspective of what can be done, as well as what may be possible with MRI, fMRI, PET and SPECT. These techniques have developed considerably since the first noisy signals were observed over a decade ago, yet significant developments are required technologically, and in methodology, interpretation and applications.

## References

1. Bandettini PA, Wong EC, Hinks RS, Tikofsky RS, Hyde JS. Time course EPI of human brain function during task activation. *Magn Reson Med* 1992; **25**: 390–7.
2. Ogawa S, Tank DW, Menon R et al. Intrinsic signal changes accompanying sensory stimulation: functional brain mapping with magnetic resonance imaging. *Proc Natl Acad Sci USA* 1992; **89**: 5951–5.
3. Kwong KK, Belliveau JW, Chesler DA et al. Dynamic magnetic resonance imaging of human brain activity during primary sensory stimulation. *Proc Natl Acad Sci USA* 1992; **89**: 5675–9.
4. Menon RS, Ogawa S, Tank DW, Ugurbil K. 4 tesla gradient recalled echo characteristics of photic stimulation – induced signal changes in the human primary visual cortex. *Magn Reson Med* 1993; **30**: 380–6.
5. Turner R, Jezzard P, Wen H et al. Functional mapping of the human visual cortex at 4 and 1.5 tesla using deoxygenation contrast EPI. *Magn Reson Med* 1993; **29**: 277–9.

6. Gati JS, Menon RS, Ugurbil K, Rutt BK. Experimental determination of the BOLD field strength dependence in vessels and tissue. *Magn Reson Med* 1997; **38**: 296–302.
7. Noll D. A primer on MRI and functional MRI (Version 2.1, 6/21/01). <http://www.bme.umich.edu/~dnoll/primer2.pdf>.
8. Lauterbur PC. Imager formation by induced local interactions. Examples employing nuclear magnetic resonance. *Nature* 1973; **242**: 190–1.
9. Mansfield P, Grannell PK. Diffraction and microscopy in solids and liquids by NMR. *Phys Rev B* 1975; **12**: 3618–34.
10. Cohen MS, Weisskoff RM. Ultra-fast imaging. *Magn Reson Imaging* 1991; **9**: 1–37.
11. Howseman AM, Grootoink S, Porter DA et al. The effect of slice order and thickness on fMRI activation data using multislice echo-planar imaging. *Neuroimage* 1999; **9**: 363–76.
12. Rosen BR, Belliveau JW, Aronen HJ et al. Susceptibility contrast imaging of cerebral blood volume: human experience. *Magn Reson Med* 1991; **22**: 293–9.
13. Rosen BR, Belliveau JW, Chien D. Perfusion imaging by nuclear magnetic resonance. *Magn Reson Quart* 1989; **5**: 263–81.
14. Belliveau JW, Kennedy DN, McKinstry RC et al. Functional mapping of the human visual cortex by magnetic resonance imaging. *Science* 1991; **254**: 716–19.
15. Williams DS, Detre JA, Leigh JS, Koretsky AS. Magnetic resonance imaging of perfusion using spin-inversion of arterial water. *Proc Natl Acad Sci USA* 1992; **89**: 212–16.
16. Detre JA, Leigh JS, Williams DS, Koretsky AP. Perfusion imaging. *Magn Reson Med* 1992; **23**: 37–45.
17. Kwong KK, Chesler DA, Weisskoff RM, Rosen BR. Perfusion MR imaging. In: Proceedings of SMR, 2nd Annual Meeting, San Francisco, 1994.
18. Wong EC, Buxton RB, Frank LR. Implementation of quantitative perfusion imaging techniques for functional brain mapping using pulsed arterial spin labeling. *NMR Biomed* 1997; **10**: 237–49.
19. Kim S-G. Quantification of relative cerebral blood flow change by flow-sensitive alternating inversion recovery (FAIR) technique: application to functional mapping. *Magn Reson Med* 1995; **34**: 293–301.
20. Ogawa S, Lee TM, Kay AR, Tank DW. Brain magnetic resonance imaging with contrast dependent on blood oxygenation. *Proc Natl Acad Sci USA* 1990; **87**: 9868–72.
21. Turner R, LeBihan D, Moonen CTW, Despres D, Frank J. Echo-planar time course MRI of cat brain oxygenation changes. *Magn Reson Med* 1991; **22**: 159–66.
22. Ogawa S, Lee TM. Functional brain imaging with physiologically sensitive image signals. *J Magn Reson Imaging* 1992; **2 (Suppl)**: S22.
23. Frahm J, Bruhn H, Merboldt K-D, Hancicke W, Math D. Dynamic MR imaging of human brain oxygenation during rest and photic stimulation. *J Magn Reson Imaging* 1992; **2**: 501–505.
24. Haacke EM, Lai S, Reichenbach JR et al. In vivo measurement of blood oxygen saturation using magnetic resonance imaging: a direct validation of the blood oxygen level-dependent concept in functional brain imaging. *Hum Brain Mapping* 1997; **5**: 341–6.
25. vanZijl PCM, Eleff SM, Ulatowski JA et al. Quantitative assessment of blood flow, blood volume, and blood oxygenation effects in functional magnetic resonance imaging. *Nature Med* 1998; **4**: 159–60.

26. Davis TL, Kwong KK, Weisskoff RM, Rosen BR. Calibrated functional MRI: mapping the dynamics of oxidative metabolism. *Proc Natl Acad Sci USA* 1998; **95**: 1834–9.
27. Kim S-G, Ugurbil K. Comparison of blood oxygenation and cerebral blood flow effects in fMRI: estimation of relative oxygen consumption change. *Magn Reson Med* 1997; **38**: 59–65.
28. Hoge RD, Atkinson J, Gill B, Crelier GR, Marrett S, Pike GB. Investigation of BOLD signal dependence on cerebral blood flow and oxygen consumption: the deoxyhemoglobin dilution model. *Magn Reson Med* 1999; **42**: 849–63.
29. Hoge RD, Atkinson J, Gill B, Crelier GR, Marrett S, Pike GB. Stimulus-dependent BOLD and perfusion dynamics in human V1. *Neuroimage* 1999; **9**: 573–85.
30. Liu TT, Luh W-M, Wong EC, Frank LR, Buxton RB. A method for dynamic measurement of blood volume with compensation for T2 changes. In: Proceedings of ISMRM 8th Annual Meeting, Denver, 2000.
31. Arthurs, OJ, Boniface, S. How well do we understand the origins of the fMRI BOLD signal? *Trends Neurosci* 2002; **25**: 27–31
32. Attwell D, Iadecola C. The neural basis of functional brain imaging signals. *Trends Neurosci* 2002; **25**: 621–5.
33. Pauling L, Coryell CD. The magnetic properties and structure of hemoglobin, oxyhemoglobin, and carbonmonoxyhemoglobin. *Proc Natl Acad Sci USA* 1936; **22**: 210–16.
34. Thulborn KR, Waterton JC, Matthews PM, Radda GK. Oxygenation dependence of the transverse relaxation time of water protons in whole blood at high field. *Biochim Biophys Acta* 1982; **714**: 265–70.
35. Yablonskiy DA. Quantitation of intrinsic magnetic susceptibility-related effects in a tissue matrix. Phantom study. *Magn Reson Med* 1998; **39**: 417–28.
36. Ogawa S, Menon RS, Tank DW et al. Functional brain mapping by blood oxygenation level-dependent contrast magnetic resonance imaging: a comparison of signal characteristics with a biophysical model. *Biophysical J* 1993; **64**: 803–12.
37. Boxerman JL, Hamberg LM, Rosen BR, Weisskoff RM. MR contrast due to intravascular magnetic susceptibility perturbations. *Magn Reson Med* 1995; **34**: 555–66.
38. Kennan RP, Zhong J, Gore JC. Intravascular susceptibility contrast mechanisms in tissues. *Magn Reson Med* 1994; **31**: 9–21.
39. Bandettini PA, Wong EC. Effects of biophysical and physiologic parameters on brain activation-induced R2\* and R2 changes: simulations using a deterministic diffusion model. *Int J Imaging Sys Technol* 1995; **6**: 134–52.
40. Weisskoff RM, Zuo CS, Boxerman JL, Rosen BR. Microscopic susceptibility variation and transverse relaxation: theory and experiment. *Magn Reson Med* 1994; **31**: 601–10.
41. Boxerman JL, Bandettini PA, Kwong KK et al. The intravascular contribution to fMRI signal change: Monte Carlo modelling and diffusion-weighted studies in vivo. *Magn Reson Med* 1995; **34**: 4–10.
42. Kim SG, Rostrup E, Larsson HB, Ogawa S, Paulson OB. Determination of relative CMRO<sub>2</sub> from CBF and BOLD changes: significant increase of oxygen consumption rate during visual stimulation. *Magn Reson Med* 1999; **41**: 1152–61.

43. An H, Lin W, Celik A, Lee YZ. Quantitative measurements of cerebral metabolic rate of oxygen utilization using MRI: a volunteer study. *NMR Biomed* 2001; **14**: 441–7.
44. Bandettini PA et al. Functional MRI using the BOLD approach: dynamic characteristics and data analysis methods. In D LeBihan (Ed) *Diffusion and Perfusion: Magnetic Resonance Imaging* (New York: Raven Press 1995) 335–49.
45. Friston KJ, Josephs O, Rees G, Turner R. Nonlinear event-related responses in fMRI. *Magn Reson Med* 1998; **39**: 41–52.
46. Josephs O, Turner R, Friston K. Event-related fMRI. *Hum Brain Mapping* 1997; **5**: 243–8.
47. Cohen MS. Parametric analysis of fMRI data using linear systems methods. *Neuroimage* 1997; **6**: 93–103.
48. Glover GH. Deconvolution of impulse response in event-related BOLD fMRI. *Neuroimage* 1999; **9**: 416–29.
49. Dale AM, Buckner RL. Selective averaging of rapidly presented individual trials using fMRI. *Hum Brain Mapping* 1997; **5**: 329–40.
50. Savoy RL, O'Craven KM, Weisskoff RM, Davis TL, Baker J, Rosen B. Exploring the temporal boundaries of fMRI: measuring responses to very brief visual stimuli. In: *Book of Abstracts, Society for Neuroscience 24th Annual Meeting*; Miami, 1994.
51. Savoy RL, Bandettini PA, Weisskoff RM et al. Pushing the temporal resolution of fMRI: studies of very brief visual stimuli, onset variability and asynchrony, and stimulus-correlated changes in noise. In: *Proceedings of SMR, 3rd Annual Meeting, Nice, 1995*.
52. Saad ZS, Ropella KM, Cox RW, DeYoe EA. Analysis and use of FMRI response delays. *Hum Brain Mapping* 2001; **13**: 74–93.
53. Buckner RL, Bandettini PA, O'Craven KM et al. Detection of cortical activation during averaged single trials of a cognitive task using functional magnetic resonance imaging. *Proc Natl Acad Sci USA* 1996; **93**: 14,878–83.
54. Lee AT, Glover GH, Meyer CH. Discrimination of large venous vessels in time-course spiral blood-oxygen-level-dependent magnetic-resonance functional neuroimaging. *Magn Reson Med* 1995; **33**: 745–54.
55. Saad ZS, DeYoe EA. Time delay estimates of FMRI signals: efficient algorithm & estimate variance. In: *Proceedings of the 19th annual international conference of IEEE/EMBS, Chicago, 1997*.
56. Binder JR, Rao SM, Hammeke TA, Frost JA, Bandettini PA, Hyde JS. Effects of stimulus rate on signal response during functional magnetic resonance imaging of auditory cortex. *Cognitive Brain Res* 1994; **2**: 31–8.
57. Rao SM, Bandettini PA, Binder JR et al. Relationship between finger movement rate and functional magnetic resonance signal change in human primary motor cortex. *J Cereb Blood Flow Metab* 1996; **16**: 1250–4.
58. Tootell RB, Reppas JB, Kwong KK et al. Functional analysis of human MT and related visual cortical areas using magnetic resonance imaging. *J Neurosci* 1995; **15**: 3215–30.
59. Disbrow EA, Slutsky DA, Roberts TP, Krubitzer LA. Functional MRI at 1.5 tesla: a comparison of the blood oxygenation level-dependent signal and electrophysiology. *Proc Natl Acad Sci USA* 2000; **97**: 9718–23.
60. Rees G, Friston K, Koch C. A direct quantitative relationship between the functional properties of human and macaque V5. *Nat Neurosci* 2000; **3**: 716–23.

61. Heeger DJ, Huk AC, Geisler WS, Albrecht DG. Spikes versus BOLD: what does neuroimaging tell us about neuronal activity? *Nat Neurosci* 2000; **3**: 631–3.
62. Logothetis N, Pauls J, Augath M, Trinath T, Oeltermann A. Neurophysiological investigation of the basis of the fMRI signal. *Nature* 2001; **412**: 150–7.
63. Boynton GM, Engel SA, Glover GH, Heeger DJ. Linear systems analysis of functional magnetic resonance imaging in human V1. *J Neurosci* 1996; **16**: 4207–21.
64. Vazquez AL, Noll DC. Nonlinear aspects of the BOLD response in functional MRI. *Neuroimage* 1998; **7**: 108–18.
65. Buxton RB, Wong EC, Frank LR. A biomechanical interpretation of the BOLD signal time course: the balloon model. In: Proceedings of the ISMRM, 5th Annual Meeting, Vancouver, 1997.
66. Frahm J, Krüger G, Merboldt K-D, Kleinschmidt A. Dynamic uncoupling and recoupling of perfusion and oxidative metabolism during focal activation in man. *Magn Reson Med* 1996; **35**: 143–8.
67. Busatto GF, Pilowsky LS. Neuroreceptor imaging with PET and SPET: research and clinical applications. In: (Kerwin R, ed) *Neurobiology and Psychiatry – Neuroimaging*. (Cambridge University Press: Cambridge, 1995) 111–24.
68. Fugita M., Innis RB. In vivo molecular imaging: ligand development and research application. In: (Davis KL, Charney D, Coyle JT, Nemeroff CB, eds) *Psychopharmacology: the Fifth Generation of Progress*. (Raven Press Ltd: New York, 2002) 411–25.
69. Meikle SR, Dahlbom M. Positron emission tomography. In: (Murray IPC, Ell PJ, eds) *Nuclear Medicine in Clinical Diagnosis and Treatment*. (Churchill Livingstone: London, 1998) 1603–16.
70. Walker B, Jarrit P. Basic physics of nuclear medicine. In: (Murray IPC, Ell PJ, eds) *Nuclear Medicine in Clinical Diagnosis and Treatment*. (Churchill Livingstone: London, 1998) 1445–58.
71. Reba RC. PET and SPECT: opportunities and challenges for psychiatry. *J Clin Psychiatry* 1993; **54**: 26–32.
72. Mallison RT. Positron and single photon emission tomography. In: (Bloom FE, Kupfer DJ, eds) *Psychopharmacology: the Fourth Generation of Progress*. (Raven Press Ltd: New York, 1994) 865–79.
73. Eberl S, Zimmerman RE. Nuclear medicine imaging instrumentation. In: (Murray IPC, Ell PJ, eds) *Nuclear Medicine in Clinical Diagnosis and Treatment*. (Churchill Livingstone: London, 1998) 1559–69.
74. Westera G, Buck A, Burger C, Leenders KL, von Schulthess GK, Schubiger AP. Carbon-11 and iodine-123 labelled iomazenil: a direct PET–SPET comparison. *Eur J Nucl Med* 1996; **23**: 5–12.
75. Pike VW. Positron-emitting radioligand for studies in vivo – probes for human psychopharmacology. *J Psychopharmacol* 1993; **7**: 139–58.
76. Halldin C, Gulyas B, Langer O, Farde L. Brain radioligands – state of the art and new trends. *Q J Nucl Med* 2001; **45**: 139–52.
77. Mintun MA, Raichle ME, Kilbourn MR, Wooten GF, Welch MJ. A quantitative model for the in vivo assessment of drug binding sites with positron emission tomography. *Ann Neurol* 1984; **15**: 217–27.

78. Laruelle M. The role of model-based methods in the development of single scan techniques. *Nucl Med Biol* 2000; **27**: 637–42.
79. Carson RE. Precision and accuracy considerations of physiological quantitation in PET. *J Cereb Blood Flow Metab* 1991; **11**: A45–A50.
80. Laruelle M, Abi-Dargham A, al Tikriti MS et al. SPECT quantification of [123I]iomazenil binding to benzodiazepine receptors in nonhuman primates: II. Equilibrium analysis of constant infusion experiments and correlation with in vitro parameters. *J Cereb Blood Flow Metab* 1994; **14**: 453–65.
81. Laruelle M, Baldwin RM, Rattner Z et al. SPECT quantification of [123I]iomazenil binding to benzodiazepine receptors in nonhuman primates: I. Kinetic modeling of single bolus experiments. *J Cereb Blood Flow Metab* 1994; **14**: 439–52.
82. Logan J, Volkow ND, Fowler JS et al. Effects of blood flow on [11C]raclopride binding in the brain: model simulations and kinetic analysis of PET data. *J Cereb Blood Flow Metab* 1994; **14**: 995–1010.
83. Lammertsma AA, Hume SP. Simplified reference tissue model for PET receptor studies. *Neuroimage* 1996; **4**: 153–8.
84. Carson RE, Channing MA, Blasberg RG et al. Comparison of bolus and infusion methods for receptor quantitation: application to [18F]cyclofoxy and positron emission tomography. *J Cereb Blood Flow Metab* 1993; **13**: 24–42.
85. Farde L, Hall H, Ehrin E, Sedvall G. Quantitative analysis of D2 dopamine receptor binding in the living human brain by PET. *Science* 1986; **231**: 258–61.
86. Carson RE. PET physiological measurements using constant infusion. *Nucl Med Biol* 2000; **27**: 657–60.
87. Innis RB, al Tikriti MS, Zoghbi SS et al. SPECT imaging of the benzodiazepine receptor: feasibility of in vivo potency measurements from stepwise displacement curves. *J Nucl Med* 1991; **32**: 1754–61.
88. Friston KJ, Price CJ, Fletcher P, Moore C, Frackowiak RSJ, Dolan RJ. The trouble with cognitive subtraction. *Neuroimage* 1996; **4**: 97–104.
89. Bandettini PA, Jesmanowicz A, Wong EC, Hyde JS. Processing strategies for time-course data sets in functional MRI of the human brain. *Magn Reson Med* 1993; **30**: 161–73.
90. Bandettini PA. *Magnetic resonance imaging of human brain activation using endogenous susceptibility contrast*. PhD Thesis, Milwaukee: Medical College of Wisconsin, 1995.
91. Engel SA, Glover GH, Wandell BA. Retinotopic organization in human visual cortex and the spatial precision of functional MRI. *Cerebral Cortex* 1997; **7**: 181–92.
92. Sereno MI, Dale AM, Reppas JR et al. Functional MRI reveals borders of multiple visual areas in humans. *Science* 1995; **268**: 889–93.
93. DeYoe EA, Carman G, Bandettini P et al. Mapping striate and extrastriate areas in human cerebral cortex. *Proc Natl Acad Sci USA* 1996; **93**: 2382–6.
94. Servos P, Zacks J, Rumelhart DE, Glover GH. Somatotopy of the human arm using fMRI. *Neuroreport* 1998; **9**: 605–9.
95. Talavage TM, Ledden PJ, Sereno MI, Benson RR, Rosen BR. Preliminary fMRI evidence for tonotopicity in human auditory cortex. *Neuroimage* 1996; **3**: S355.
96. Zarahn E, Aguirre G, D'Esposito M. A trial-based experimental design for fMRI. *Neuroimage* 1997; **6**: 122–38.

## NEUROIMAGING IN PSYCHIATRY

97. Clark VP, Maisog JM, Haxby JV. fMRI study of face perception and memory using random stimulus sequences. *J Neurophysiol* 1998; **79**: 3257–65.
98. Dale A, Buckner R. Selective averaging of individual trials using fMRI. In: Third International Conference on Functional Mapping of the Human Brain, Copenhagen, 1997.
99. McCarthy G, Luby M, Gore J, Goldman-Rakic P. Infrequent events transiently activate human prefrontal and parietal cortex as measured by functional MRI. *J Neurophysiol* 1997; **77**: 1630–4.
100. Schacter DL, Buckner RL, Koutstaal W, Dale AM, Rosen BR. Late onset of anterior prefrontal activity during true and false recognition: an event-related fMRI study. *Neuroimage* 1997; **6**: 259–69.
101. Dale AM. Optimal experimental design for event-related fMRI. *Hum Brain Mapping* 1999; **8**: 109–14.
102. Burock MA, Buckner RL, Woldorff MG, Rosen BR, Dale AM. Randomized event-related experimental designs allow for extremely rapid presentation rates using functional MRI. *Neuroreport* 1998; **9**: 3735–9.
103. Liu TT, Frank LR, Wong EC, Buxton RB. Detection power, estimation efficiency, and predictability in event-related fMRI. *Neuroimage* 2001; **13**: 759–73.
104. Birn RM, Cox RW, Bandettini PA. Detection versus estimation in event-related fMRI: choosing the optimal stimulus timing. *Neuroimage* 2002; **15**: 252–64.
105. Courtney SM, Ungerleider LG, Keil K, Haxby JV. Transient and sustained activity in a distributed neural system for human working memory. *Nature* 1997; **386**: 608–11.
106. Patterson J, Bandettini P, Ungerleider LG. Simultaneous skin conductance measurement and fMRI during cognitive tasks: correlations of skin conductance activity with ventromedial prefrontal cortex (PFC) and orbitofrontal cortex (OFC) activity. In: Proceedings of Human Brain Mapping, San Antonio, 2000.
107. Shergill SS, Bullmore E, Simmons A, Murray R, McGuire P. Functional anatomy of auditory verbal imagery in schizophrenic patients with auditory hallucinations. *Am J Psychiatry* 2000; **157**: 1691–3.